UDC 551.513.1:551.511.33:551.509.313(213)

Response of the Tropical Atmosphere to Local, Steady Forcing

PETER J. WEBSTER [1]—*Massachusetts Institute of Technology, Cambridge, Mass.*

ABSTRACT—A theoretical analysis is made of the large-scale, stationary, zonally asymmetric motions that result from heating and the orographic effect in the tropical atmosphere. The release of latent heat dominates the sensible and radiational heating and the latter two effects are ignored. The first linear model is a continuous stratified atmosphere in solid westward rotation with no dissipation. Of all the modes, only the rotationally trapped Kelvin wave exhibits a significant response. Because the Kelvin wave response does not compare well with the observed flow, we concluded that the neighboring westerlies in the real atmosphere are important even if the forcing is in low latitudes.

The second linear model is a two-layer numerical model including parameterized dissipation and realistic basic currents. Realistic forcing is considered, following an analysis of the response to especially simple forms of heating and orographic forcing. Dissipative effects close to the Equator are very important in this model. The dominant forcing at very low latitudes is the latent heating; at higher latitudes, the advective terms and the effects of rotation become more important and the influences of orography and heating are more nearly equal. A study of the energetics shows that the response near the Equator is due to both local latent heating and the effect of steady, forced motions at subtropical latitudes.

Comparison of the response of the model with observed motion fields and with the results of other studies suggests that most of the time-independent circulation of low latitudes is forced by heating and orography within the Tropics and subtropics. In the subtropics, however, forcing from higher latitudes must be of importance.

1. INTRODUCTION

During the last decade or so, the role of the tropical atmosphere in the general circulation has been a topic of great interest and some debate. Much of this debate has emanated from two differing theories as to how the tropical atmosphere is driven. The first avenue of thought centers on the idea that the low-latitude condensation processes constitute the principal driving force of the tropical atmosphere (Riehl 1965, Manabe and Smagorinsky 1967), while the second theory considers lateral coupling with higher latitude energy sources as the most important driving force of the Tropics (Mak 1969). Charney (1969) suggested that a combination of both mechanisms is likely, and recently Manabe et al. (1970) reconciled the differences between the two theories using a numerical simulation study of the tropical atmosphere.

From analyses of wind data in the lower stratosphere over the equatorial Pacific Ocean, the existence of transient planetary-scale waves were first identified by Yanai and Maruyama (1966). Since then, these transient modes have been the subject of many observational and theoretical studies (e.g., Matsuno 1966, Lindzen 1967, Mak 1969, and many others). Except for the numerical study of Manabe et al. (1970), most investigations of the steady (or time-independent) circulations are of an observational nature. Kidson et al. (1969) studied the statistical properties of both the steady and transient large-scale equatorial motions using many years of conventional data. More recently, a detailed description of the mean fields of motion at low latitudes for June, July, and August of 1967 has been undertaken by Krishnamurti (1970), who was able to supplement the conventional data coverage with aircraft wind observations. Other observational studies exist, but these tend to refer to some specific phenomenon in a specific region (e.g., the study of the easterly jet stream over the Indian Ocean by Koteswaram 1958, Flohn 1964). With the exceptions mentioned above, the structure of the stationary circulations in low latitudes has received relatively little attention.

Figure 1 shows the spatial deviations of the time-averaged zonal and meridional velocity components at the Equator. The components are represented at specific pressure levels for the two seasons, December, January, and February (DJF) and June, July, and August (JJA). Both components possess appreciable variation in both longitude and height. Especially interesting is the height variation. For example, in each season, both components possess minima in the middle troposphere and maxima in the upper and lower troposphere. Furthermore, the motions in the lower levels appear to be almost completely out of phase with the motions at 200 mb.

What mechanisms can be responsible for the stationary disturbances shown in figure 1? One possibility is the forcing of equatorial motions by standing eddies of higher latitudes in a manner similar to that described by Mak (1969) for the transient eddies. Other possibilities also exist. Three continents straddle the Equator—South America, equatorial Africa, and the maritime "continent" of Indonesia—each with considerable orography. The northern sector of the Tropics contains the arid regions

[1] Now at the Department of Meteorology, University of California, Los Angeles

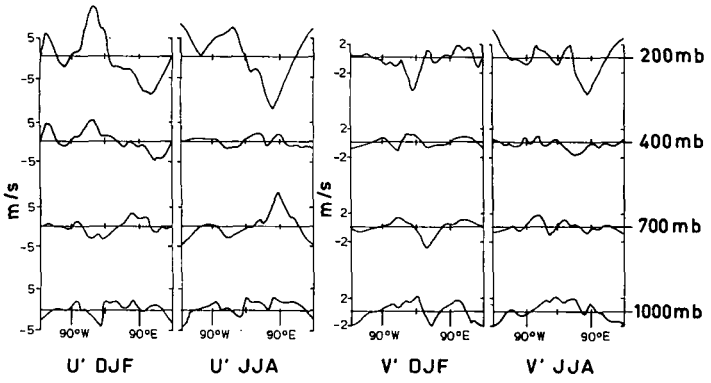

FIGURE 1.—Observed values of the spatial deviation of the time-averaged velocity fields along the Equator for the two seasons, DJF and JJA. The zonal and meridional components (U' and V', respectively) are shown at the indicated pressure levels.

of the Sahara and the Middle East, the Indian subcontinent, and the Himalayan Mountains. The annual distribution of precipitation in the Tropics reveals a large longitudinal variation. For example, each of the three tropical continents possesses relative precipitation maxima, the possible importance of which has been discussed by Ramage (1968). It thus seems that the orography, the release of latent heat, the effect of the ocean–continental contrast, and perhaps a longitudinal radiational heating variation could play a role in the production of the standing eddies. The purpose of this study is to assess the role played by these forcing functions located within the Tropics.

Specifically, this study is a theoretical attempt to investigate the large-scale, stationary, zonally asymmetric motions that result from the influence of forcing functions *within* the tropical atmosphere. The importance of forcing from higher latitudes is also discussed.

In midlatitudes, the study of steady motions generated by longitudinally dependent forcing has a long history going back at least to Rossby's (1939) surmise on the excitation of the free modes of a simple atmosphere. Charney and Eliassen (1949) were the first to make a detailed study of the perturbation of the westerlies by orography. They were soon followed by Smagorinsky (1953), who considered the effect of zonally asymmetric external heating. Since these pioneering works, there has been a multitude of similar steady-state models that have been fairly successful in reproducing at least the gross features of the midlatitude stationary flow.

The above studies were all steady-state linear boundary value problems. A second form of model instigated by Phillips (1956) consists of starting with some prescribed initial state and predicting its evolution over a long period of time. The time-averaged solution is considered to be the climate of the model. Such models have become very sophisticated and now extend over the entire globe and include many levels in the vertical. The numerical methods of solution allow the incorporation of various physical processes such as the release of latent heat through a complete hydrology cycle (e.g., Manabe et al. 1970). Although such complicated feedback mechanisms may be incorporated into the model, it is a difficult and costly task to study one particular process or phenomenon.

In the ensuing study, our philosophy will be to make the models simple enough for mathematical tractability while still retaining as many of the features of the tropical atmosphere as we can. The price we pay for this is the simplicity with which we must represent the forcing functions. For example, it will be necessary to introduce the orographic forcing as a simple boundary condition at the lower boundary of the model. Then, rather than allowing the motions to interact and determine the latent heat release, we are forced to seek the circulation that is consistent with a known forcing function. The problems involved in representing the forcing functions in this manner will be discussed in the next section.

2. FORCING FUNCTIONS AT LOW LATITUDE

Since the topography of the earth's surface is well known, the determination of the orography function presents little problem. The resolution of the heating functions, however, is a much more difficult task. Such functions cannot be measured directly; therefore, a relationship between the function and some other observable field(s) must be known. Even if we know the relationship well, we have to cope with the observational problem, which is especially acute in equatorial regions. To overcome this observational problem, we will make use of satellite data to determine at least the gross features of the major low-latitude heat sources and sinks.

Being primarily interested in the response of the tropical atmosphere to localized forcing, we will assume that the forcing functions decay exponentially poleward of 30° latitude according to the law

$$f(\theta)=\exp\left[-10(\sin\theta-0.3)^2\right] \tag{1}$$

so that orographic or heating functions, $\chi(\theta,\varphi)$, may be written as

$$\begin{aligned} &\chi(\theta,\varphi)=\chi(\theta,\varphi) && |\theta|\leq 30^\circ \\ \text{and}\quad &\\ &\chi(\theta,\varphi)=\chi(\theta=30^\circ,\varphi)f(\theta) && |\theta|>30^\circ. \end{aligned} \tag{2}$$

The reverse problem, that of the influence of steady forcing from midlatitudes upon the tropical region, will be discussed later.

Orography

To form the orographic function, we used the estimates of Berkofsky and Bertoni (1955). From their 5° average elevations, values every 10° of longitude and 5° of latitude between ±30° latitude were extracted. This produced the array $h(\theta,\varphi)$.

The orography function is conveniently represented in wave-number space. To do this, we expand the orography in the Fourier series

$$h(\theta,\varphi)=\sum_{s=0}^{\infty}\left[h_R^s(\theta)\cos s\varphi+h_I^s(\theta)\sin s\varphi\right] \tag{3}$$

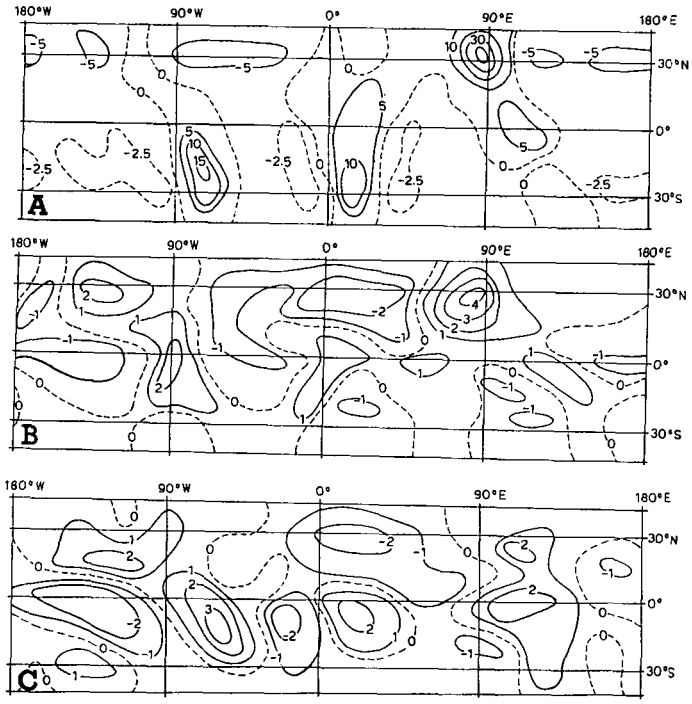

FIGURE 2.—Composite map of (A) the orography (10^2 m), (B) the DJF latent heating (10^{-2} cal·cm^{-2}·day^{-1}), and (C) the JJA latent heating using the first nine nonzero Fourier coefficients.

where $h_R^s(\theta)$ and $h_I^s(\theta)$ are the real sth cosine and sine coefficients, respectively, and s is a non-negative integer.

Figure 2A illustrates the recomposition of the orography with the first nine harmonics, except $s=0$. Four features predominate. These are the Andes, the African highlands, the mountains of the maritime continent Indonesia, and the Himalayan Mountains. In forming the orographic forcing function, we will only use the first nine longitudinal harmonics, as the inclusion of the higher wave numbers tends only to "sharpen" the existing peaks and "smooth" the surface of the ocean.

Heating

Heating and cooling of the atmosphere involves many complicated processes. In the simplest sense, we may represent the total heating in a unit column (cal·cm^{-2}·day^{-1}) as

$$\mathcal{Q}_{\text{TOTAL}}=(\mathcal{Q}_{\text{SW}}+\mathcal{Q}_{\text{LW}})+\mathcal{Q}_{\text{SEN}}+\mathcal{Q}_{\text{LH}} \qquad (4)$$

where $\mathcal{Q}_{\text{SW}}$ represents the absorption of solar short-wave radiation in the column, $\mathcal{Q}_{\text{LW}}$ is the long-wave emission, $\mathcal{Q}_{\text{SEN}}$ is the heating or cooling by the turbulent transfer of sensible heat between the atmosphere and its lower boundary, and $\mathcal{Q}_{\text{LH}}$ is the heating or cooling due to the condensation or evaporation of water vapor.

The complexity of investigating the heat budget of the earth-atmosphere system or estimating those heating functions likely to be of importance in our study is exemplified by the interdependency of the various terms in eq (4). For example, the large release of latent heat in the tropical atmosphere is likely to be dependent upon, at least initially, an equatorial flux of moist air forced by a mean north–south radiation heating gradient. Also, the preferred longitudinal distribution of precipitation in the Tropics (and hence the release of latent heat) appears to be coupled to the sensible heat flux at the lower boundary. An example of this interdependency is the cloudless region of the equatorial southeastern Pacific Ocean that coincides with the cold oceanic upwelling areas.

TABLE 1.—*Zonal mean and zonal rms values of the various heating functions (cal·cm^{-2}·day^{-1}). Calculations were made using the estimates of Katayama (1964)*

Lat.	0°	10°N	20°N	30°N
		January		
$\mathcal{Q}_{\text{RAD}}$	−210± 12	−255± 25	−238± 24	−216± 26
$\mathcal{Q}_{\text{SEN}}$	6± 24	7± 22	26± 20	39± 24
$\mathcal{Q}_{\text{LH}}$	288±110	196±111	83± 80	118± 80
$\mathcal{Q}_{\text{TOTAL}}$	83±112	−18±113	−100± 88	−35± 95
		July		
$\mathcal{Q}_{\text{RAD}}$	−192± 19	−183± 24	−185± 23	−175± 27
$\mathcal{Q}_{\text{SEN}}$	10± 18	11± 28	32± 40	63± 55
$\mathcal{Q}_{\text{LH}}$	256±112	354±139	232±192	157±166
$\mathcal{Q}_{\text{TOTAL}}$	74±108	185±152	88±198	57±180

Unfortunately, the linear aspects of our study do not allow the treatment of the interdependency and full complexity of the terms in eq (4). Rather, we can, at best, treat these processes as separate entities and estimate their relative importance. To do this, we will utilize earlier atmospheric heat budget studies.

From Katayama (1964), we have mean estimates of the terms of eq (4) for January and July over the Northern Hemisphere. Using these results, the zonal average and root-mean-square (rms) value of each term was calculated at 0°, 10°N, 20°N, and 30°N for both months. The results are displayed in table 1.

Considering the rms values of the various terms, we note that the longitudinal variation of $\mathcal{Q}_{\text{RAD}}$ (where $\mathcal{Q}_{\text{RAD}}=\mathcal{Q}_{\text{SW}}+\mathcal{Q}_{\text{LW}}$) and $\mathcal{Q}_{\text{SEN}}$ is appreciably smaller than $\mathcal{Q}_{\text{LH}}$. In fact, latent heat accounts for nearly all the total variance. Thus, in choosing the most important terms of eq (4), we must relegate the longitudinal variation of $\mathcal{Q}_{\text{SEN}}$ and $\mathcal{Q}_{\text{RAD}}$ to a position of secondary importance, both individually and cumulatively, in comparison to $\mathcal{Q}_{\text{LH}}$.

Distribution of Latent Heat

Because most estimates of the distribution of the release of latent heat utilize an observed distribution of precipitation (e.g., Katayama 1964), one must devise an alternative method of determination for the Tropics that shows no bias between oceanic and continental regions.

In an attempt to achieve this goal, we assumed a direct relationship between cloudiness and precipitation (and so latent heat release). Some credence is given to this assumption by Johnson (1969), who found a high correlation between the average precipitation and cloudiness over

a region of Bangladesh (formerly East Pakistan) during a 3-mo period of the 1967 monsoon season. Estimates of cloudiness were obtained from the digitized "brightness" or mean global, visual, albedo satellite charts compiled by Taylor and Winston (1968). To allow the brightness charts to be representative of cloudiness, we first delineated the bright *cloudless* areas over the desert regions using climatological data. Such areas were relegated to the lowest brightness index. We evaluated the factor of proportionality by correlating the zonal average cloudiness with the zonal average of the latent heat release from Katayama (1964). Thus, an error in Katayama's estimate obtained from conventional data results only in an error in magnitude and not in distribution in our heating function.

In the above determination, we assumed that the background albedo of the land and ocean surfaces is the same. However, Budyko (1955) estimates that the albedos are approximately 7 percent and 15 percent, respectively, thereby slightly overestimating the latent heat release over land. Correcting for this error is a difficult task. One cannot simply reduce the latent heat estimates over land by some appropriate amount without equally affecting areas where the background reflection is unimportant, such as areas of high mean cloudiness.

Following the same procedure as with the orography function, we expand the latent heating field in the Fourier series

$$\mathcal{Q}_{LH}(\theta,\varphi)=\sum_{s=0}^{\infty}\left[q_R^s(\theta)\cos s\varphi+q_I^s(\theta)\sin s\varphi\right] \qquad (5)$$

where q_R^s and q_I^s are the sth real sine and cosine coefficients.

Figures 2B and 2C represent the recomposition of the seasonal latent heat distribution using the first nine nonzero coefficients of eq (5) and comprise spatial deviations (or perturbations) about the zonal mean. In DJF, three large maxima are apparent; these correspond roughly with the equatorial regions of South America (particularly the Amazon Basin), southern equatorial Africa, and the Indonesian region. [Ramage (1968) discussed the importance of the tropical continents as major sources of latent heat.] Arid North Africa and the Middle East appear as negative anomalies (or relative cooling regions) as do the southern Atlantic Ocean and the southeastern Pacific Ocean. Considering the JJA recomposition, we note the dominance of the extremely strong heat source in the vicinity of the Indian subcontinent. Relatively weak maxima are to be found in Africa and in the north and central parts of equatorial South America.

The southwestward extension of the latter maximum underlines a possible weakness in the scheme used to evaluate $\mathcal{Q}_{LH}$. In assuming that a direct proportionality exists between cloudiness and latent heat release, we have made the tacit assumption that cloudiness is proportional to precipitation. This assumption is perhaps better in the tropical atmosphere than elsewhere as cumulus is the predominant cloud type. However, from climatological precipitation data, the region mentioned above is particularly dry and the relatively high $\mathcal{Q}_{LH}$ value is a result of persistent nonprecipitating cloud cover.

The latent heat distributions will enter the equations of our models as steady-state or time-independent heating functions. But should one interpret the functions as constant regions of relative heating? On a day-to-day basis, we find that most precipitation results from transient disturbances of various time and space scales. More correctly, then, we should think of the latent heat fields as the time-averaged effect of these disturbances.

How much confidence may we have in these estimates? To test them, we compared selected areas of relatively well-known precipitation distribution with the seasonal latent heat determinations. The calculations, summarized in appendix 1, result in fairly good agreement between the implicit and explicit determinations.

3. SIMPLIFIED CONTINUOUS MODEL

In this section, we will consider a simple linearized model that retains some important features of the real atmosphere. To facilitate separation of the basic equations, we chose a mean state in which the basic zonal flow is one of solid rotation. That is, we let

$$\overline{U}(\theta)=\delta a\Omega\sin\theta \qquad (6)$$

where θ represents colatitude, δ is some nondimensional number, a is the radius of the earth, Ω is the angular velocity of rotation of the earth, and $\overline{U}$ is the basic zonal flow. For a westward flow of 5 m/s at the Equator, $\delta=-10^{-2}$. The mean temperature is allowed to vary only with height, and both the basic and perturbation states are assumed to be hydrostatic. For simplicity, radiational and frictional dissipative effects are ignored.

Governing Equations

The governing equations arise from the spherical primitive equations in (θ, φ, $Z=\ln p/p_0$) coordinates as given by Phillips (1963). Here, p represents pressure, p_0 is some constant, and φ is longitude. The solutions are linearized about a basic state defined by eq (6). Assuming steady-state solutions (i.e., $\partial/\partial t=0$), we derive the following linear set:

$$\delta\Omega\frac{\partial u}{\partial\varphi}-2\Omega\cos\theta(1+\delta)v=-\frac{1}{a\sin\theta}\frac{\partial\psi}{\partial\varphi},$$

$$\delta\Omega\frac{\partial v}{\partial\varphi}+2\Omega\cos\theta(1+\delta)u=\frac{1}{a}\frac{\partial\psi}{\partial\theta},$$

$$\left(\frac{\partial}{\partial Z}-1\right)\dot{Z}+\frac{1}{a\sin\theta}\frac{\partial u}{\partial\varphi}-\frac{1}{a\sin\theta}\frac{\partial}{\partial\theta}(v\sin\theta)=0,$$

$$\delta\Omega\frac{\partial}{\partial\varphi}\left(\frac{\partial\psi}{\partial Z}\right)+\dot{Z}\overline{S}(Z)=\kappa\mathcal{Q}(\theta,\varphi,Z),$$

and (7)

$$a\overline{U}\left(2\Omega\cos\theta+\frac{1}{a}\overline{U}\cot\theta\right)=\frac{\partial\overline{\Psi}}{\partial\theta}$$

where $\kappa=R/c_p$ and $\overline{S}(Z)=(\partial/\partial Z)\ [\partial\overline{\Psi}/\partial Z+(\kappa\overline{\Psi})]$. The symbols u, v, and $\dot{Z}$ represent the zonal, meridional, and vertical components of the perturbation velocity field, and ψ and $\overline{\Psi}$ are the perturbation and mean geopotential heights, respectively. $\mathcal{Q}$ is the heating rate per unit mass.

The longitudinal variation is separated out by assuming that

$$u, v, \dot{Z}, \psi(\theta, \varphi, Z)=\mathrm{Rl}\sum_s \frac{U^s}{\sin\theta}, \frac{-iV^s}{\sin\theta}, -iW^s, \Psi^s(\theta, Z)\exp(is\varphi) \tag{8a}$$

and

$$h(\theta, \varphi), \mathcal{Q}(\theta, \varphi, Z)=\mathrm{Rl}\sum_s h^s(\theta), q^s(\theta, Z)\exp(is\varphi) \tag{8b}$$

where $h^s=h_R^s-ih_I^s$ and $q^s=q_R^s-iq_I^s$ via eq (8b), (3), and (5). The term, s, is a non-negative integer, $i^2=-1$, and Rl signifies the real part of the expansion.

Nondimensionalizing, using a and $(2\Omega)^{-1}$ as the length and time scales, and introducing eq (8) into eq (7) produces the following linear relationships between the coefficient functions of μ, Z, and s. These are

$$-\lambda_s U^s+A\mu V^s+s\Psi^s=0, \tag{9a}$$

$$-\lambda_s V^s+A\mu U^s+D(\Psi^s)=0, \tag{9b}$$

$$-sU^s+D(V^s)+(1-\mu^2)P(W^s)=0, \tag{9c}$$

and

$$\lambda_s\frac{\partial\Psi^s}{\partial Z}+\overline{S}(Z)W^s=q^s(\mu,Z) \tag{9d}$$

where $\mu=\cos\theta$, $D=(1-\mu^2)(\partial/\partial\mu)$, $P=(\partial/\partial Z)-1$, $A=1+\delta$, and

$$\lambda_s=-\delta_s/2. \tag{10}$$

The term, λ_s, the apparent or "Doppler-shifted" frequency of the motions (i.e., the frequency of the various modes referred to a frame moving with the basic current), is positive for easterly flow ($\delta<0$) and negative for westerly flow ($\delta>0$).

By straightforward elimination, eq (9) is reduced to a single second-order equation in $W^s(\mu,Z)$. That is,

$$\overline{S}(Z)\mathcal{F}(W^s)-\frac{\partial}{\partial Z}P(W^s)=\mathcal{F}(q^s) \tag{11}$$

where

$$\mathcal{F}=\frac{1}{m(\mu)}\left\{\frac{\partial}{\partial\mu}D+\frac{1}{m(\mu)}\left[2A\mu D+\frac{sA}{\lambda_s}m(\mu)\right]-\frac{s^2}{1-\mu^2}\right\}$$

and

$$m(\mu)=\lambda_s^2-A^2\mu^2. \tag{12}$$

$\mathcal{F}$, the "traditional" Hough operator, is shown by Flattery (1967) to be self-adjoint, which infers its possession of real eigenvalues and orthogonal eigenfunctions.

If $W_{n,s}^*$ is the nth eigenfunction of $\mathcal{F}$ such that

$$\mathcal{F}[W_{n,s}^*(\mu)]+E_{n,s}W_{n,s}^*(\mu)=0 \tag{13}$$

where the $E_{n,s}$ are the associated eigenvalues, we can expand $W^s(\mu, Z)$, $h^s(\mu)$, and $q^s(\mu, Z)$ in these eigenfunctions. That is,

$$W^s(\mu, Z), q^s(\mu, Z), h^s(\mu)=\sum_n \beta_{n,s}(Z), J_{n,s}(Z), b_{n,s}W_{n,s}^*(\mu). \tag{14}$$

Then, between eq (13) and (14), we can separate eq (11) yielding the vertical structure equation,

$$\left(\frac{d^2}{dZ^2}+m^2\right)Y_{n,s}(Z)=E_{n,s}J_{n,s}(Z)\exp\left(\frac{Z}{2}\right) \tag{15}$$

where

$$m^2(Z)=S(Z)E_{n,s}-\tfrac{1}{4}$$

and

$$Y_{n,s}(Z)=\beta_{n,s}\exp\left(-\frac{Z}{2}\right). \tag{16}$$

Eigenfunctions and Eigenvalues

The problem is to find $W_{n,s}^*(\mu)$. We do not seek its general form, however, but only that form defined by the parameters of our very specific problem. These are $\overline{U}$ (and hence δ) and s, which together define λ_s. In appendix 2, we show that these parameters define specific ranges of magnitudes for the eigenvalues that are then used to obtain the appropriate forms of $W_{n,s}^*(\mu)$.

The Free Regime

An investigation of the free regime allows us to anticipate the reaction of the model to forcing. Similar discussions have been given for the $E>>0$ free modes by Matsuno (1966) and Lindzen (1967). Our approach differs in that we seek only to illuminate the forcing problem.

The latitudinal equation [eq (45)] represents four modal families. These modes are, respectively, a set of westward propagating Rossby waves, R, easterly and westerly propagating gravity waves, GE and GW, and an eastward moving Kelvin wave, K. In an easterly basic flow, only the eastward propagating GE and K modes are capable of being excited by stationary forcing functions. R and GW are thus ignored. A summary of the properties of the remaining stationary free modes is given below.

1. For an isothermal atmosphere and any realistic value of $\overline{S}(Z)$, m^2 in eq (16) is positive due to the large size of E. This means that all free solutions of eq (15) are vertically propagating waves and m may be considered to be the vertical wave number of the mode.

2. The vertical wavelength (defined by $2\pi/m$) of all the GE modes is extremely small and varies from the order of a meter for small s to the order of a kilometer for large s. The vertical scale of the Kelvin wave is about 1.5 km for all s.

3. The latitudinal scale of the GE modes [defined as the point where the solution of eq (45) changes from oscillatory to exponentially decaying; i.e., $\mu_c=A^{-1/2}E^{-1/4}(2n+1)^{1/2}$] falls within a degree or so of the Equator. Furthermore, one can show that, for a given s, a limiting critical latitude ($\mu_c=\lambda_s/A$) exists as $n\to\infty$. The e-folding scale of the symmetric Kelvin wave is $\pm 7°$ of latitude.

Because of the limited latitudinal extent of the $E>>0$ eigenfunctions, they cannot represent the response of the tropical atmosphere at any distance from the Equator. The remainder of the representation must lie with the eigenfunctions associated with the negative eigenvalues. These functions possess maxima in the vicinity of the poles and, for the range of negative eigenvalues defined by our problem (Longuet-Higgins 1968), decrease slowly in amplitude equatorward. However, in representing the basic state of the atmosphere by a simple easterly flow everywhere, we are making the tacit assumption that the

forcing functions, and hence the response, can be nearly represented by these modes having small amplitude at high latitudes. Since we need to consider the eigenfunctions for $E<0$, the assumption is rather weak.

Except very close to the Equator, those modes associated with the westerly wind regime adjoining the equatorial easterlies are more likely to be of greater importance. Modes associated with $\lambda_s<0$ (i.e., R and GW) may then be excited. Before incorporating a more realistic basic field, we will briefly consider the response of the Kelvin mode. Besides possibly being the only important mode of the $E>>0$ family at very low latitudes, it will aid us in the interpretation of subsequent results of the more complicated model. The response of the GE mode will be ignored since, in addition to the properties mentioned in items 2 and 3 above, its magnitude is at least two orders of magnitude smaller than that of the Kelvin wave in the small to moderate s range.

The Kelvin Wave Response

The Kelvin wave solutions are given by eq (53) and (54), subject to the appropriate boundary conditions. At $Z=\infty$, we insist that all energy is outgoing while, at $Z=0$, the boundary condition is given by the linear relationship

$$\dot{Z}=\frac{g}{RT}\left(\frac{\overline{U}}{a\sin\theta}\frac{\partial h(\theta,\varphi)}{\partial\varphi}\right)_{Z=0}.$$

By introducing eq (8), (14), and (16), we can show that

$$Y_{n,s}(Z=0)=\lambda_s\hat{b}_{n,s} \tag{17}$$

where the $\hat{b}_{n,s}$ represent the complex conjugates of the coefficients of eq (14).

A maximum latent heat release near 5 km, in keeping with the determinations of Vincent (1969), is obtained by choosing a functional form of $f(Z)=Z\exp(-1.62\ Z)$. Using eq (5), (9), and (14), we may write the heating function as

$$J_{n,s}(Z)=-i\hat{q}_{n,s}Z\exp(-1.62Z) \tag{18}$$

where the $\hat{q}_{n,s}$ are the complex conjugates of the coefficients of eq (14). The coefficient families, $\hat{b}_{n,s}$ and $\hat{q}_{n,s}$, are found from the transform of eq (14).

Using eq (17) and (18), we can determine the solutions of eq (15) for the Kelvin wave response to orography (no heating) and thermal forcing (no orography). They are, respectively,

$$Y_s(Z)=\lambda_s b_{-1,s}\exp(-imZ) \tag{19}$$

and

$$Y_s(Z)=\left(Z-\frac{2\alpha}{m^2+\alpha^2}\right)\frac{Eq}{m^2+\alpha^2}\exp(\alpha Z)+\frac{2\alpha}{(m^2+\alpha^2)^2}Eq\exp(-imZ) \tag{20}$$

where $a=1.12$.

Substituting eq (19) and (20) into the eigensolutions [eq (53) and (54)], plus the expansion coefficients of the three families of forcing functions, gives the three-dimensional response of the Kelvin wave. Figures 3–5 show cross-sections of the perturbation zonal velocity response to the DJF and JJA seasonal heating and orography, respectively, along the Equator.

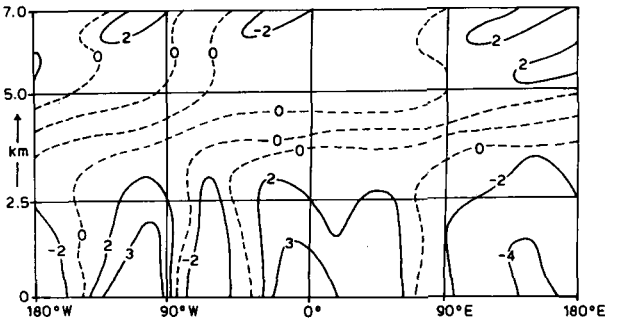

FIGURE 3.—Vertical cross-section along the Equator of the perturbation zonal current response (m/s) of the Kelvin wave due to forcing by the DJF latent-heat forcing function shown in figure 2B.

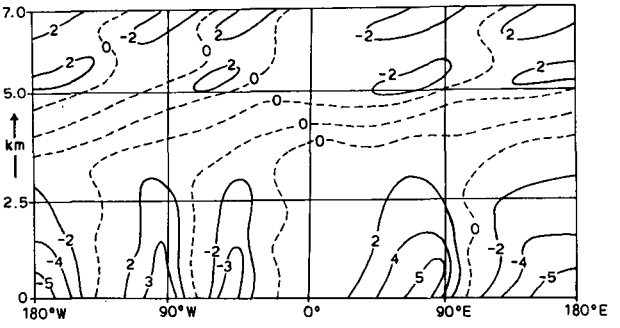

FIGURE 4.—Same as figure 3 for the JJA latent-heat forcing function shown in figure 2C.

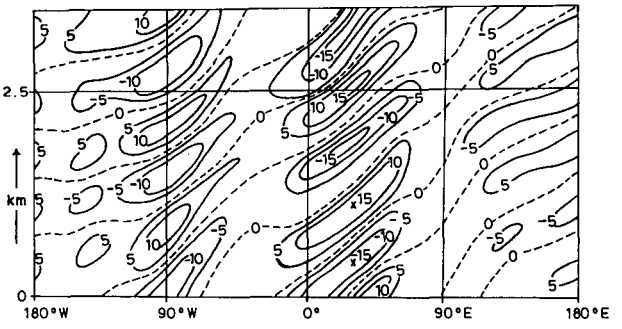

FIGURE 5.—Same as figure 3 for the orographic forcing function shown in figure 2A.

The fields of figures 3 and 4 are both characterized by regions of converging and diverging zonal currents associated, respectively, with ascending and descending air over the heat sources and sinks. Since $V=0$, the resulting flow consists of zonal or longitudinal circulations in the (φ, Z) plane with rising motion in the western parts of the ocean and subsidence in the east. This flow pattern corresponds to the circulations discussed by Bjerknes (1969). Above this region, the response changes to one characterized by a vertical circulation scale on the order of a kilometer. This corresponds to the internal gravity part of the solution.

Comparing these results with figure 1, one sees some similarity in the lower levels where the westerlies centered near 90°W, 20°E, and 90°E are roughly simulated, although the strong westerlies near 140°E in JJA are not predicted. At higher levels, the observed phase change is not apparent.

The most outstanding feature of the orographic forcing (fig. 5) is the magnitude of the response. As we shall see later, this is due to the neglect of dissipative processes in the model. The importance of dissipation to the steady-state structure of the tropical atmosphere will become apparent when we compare these results with those of the more complicated model.

4. FORMULATION OF A MORE REALISTIC MODEL

To facilitate the study of the response of a more complicated, spherical, and hydrostatic basic atmosphere, we formulated a two-layer model. Such a model represents the simplest prototype of the atmosphere capable of possessing both horizontal and vertical shear in the basic state. The complexity of the basic fields and the numerical techniques needed to solve the equations make it a difficult task to employ a radiation condition at the upper boundary. We will assume that the upper boundary is rigid, although at this stage we must question the validity of such an approximation.

As shown by the quasi-geostrophic considerations of Charney and Drazin (1961), the rigid lid condition is considered to be a good approximation when modeling midlatitude tropospheric motions. However, in low latitudes, these arguments are not valid. In a recent study of the maintenance of the quasi-biennial oscillation, Lindzen (1970) found that at certain levels the vertical propagation of equatorial waves was impeded. At such levels, the phase speed of the waves matched the basic flow. For time-independent waves (zero frequency), such critical levels occur where basic flow is zero. If such a surface did exist in the basic tropical atmosphere, it would provide an appropriate location for our rigid lid and would somewhat justify its inclusion. From the 6-yr zonal averages of Kidson et al. (1969), there appears to be little evidence of a zero surface at low latitudes; there is, instead, easterly flow through the stratosphere. However, as we will show in section 5, the importance of frictional dissipation in low latitudes suggests that for steady motions the assumption is inconsequential.

Another feature of our two-layer formulation is the simplification of the basic stratification. First, the stratification is allowed to be a function of height only, thus being represented by one value at the midpoint of the model. Second, as a consequence of the assumed horizontal independence, one must be satisfied with a mean horizontal static stability. From Dickinson (1969, fig. 4), we see that the last assumption is fairly good; there is little variation of the static stability at 500 mb between 30°N and 30°S.

Governing Equations of the Two-Layer Model

The nonlinear spherical equations in pressure coordinates (Thompson 1961) are linearized relative to a basic state defined by

$$\overline{U}(\mu, p)=(1-\mu^2)^{1/2}a\Omega\delta(\mu, p) \tag{21}$$

where $\delta(\mu, p)$ is some nondimensional function to be determined.

Introducing a, $(2\Omega)^{-1}$ and $p_0=1000$ mb as the length, time, and pressure scales, we derive the following linear, hydrostatic, and spherical primitive equations:

$$\Delta\frac{\partial u'}{\partial\varphi}+(1-\mu^2)v'\frac{\partial\Delta}{\partial\mu}+(1-\mu^2)\omega\frac{\partial\Delta}{\partial p}$$

$$-\mu v'(2\Delta+1)=-\frac{\partial\psi}{\partial\varphi}+(1-\mu^2)^{1/2}F_\varphi, \tag{22a}$$

$$\Delta\frac{\partial v'}{\partial\varphi}+\mu u'(2\Delta+1)=-D(\psi)+(1-\mu^2)^{1/2}F_\mu, \tag{22b}$$

$$\frac{\partial u'}{\partial\varphi}+(1-\mu^2)\left(\frac{\partial\omega}{\partial p}+\frac{\partial v'}{\partial\mu}\right)=0, \tag{22c}$$

$$\Delta\frac{\partial}{\partial\varphi}\left(\frac{\partial\psi}{\partial p}\right)+v'\frac{\partial}{\partial\mu}\left(\frac{\partial\overline{\Psi}}{\partial p}\right)+\frac{\omega}{p^2}\overline{S}(p)=-\frac{\dot{Q}}{p}, \tag{22d}$$

and

$$\frac{\partial\overline{\Psi}}{\partial\mu}=-\Delta(1+\Delta)\mu \tag{22e}$$

where $\Delta(\mu, p)=\delta/2$, $u'=(1-\mu^2)^{1/2}u$, $v'=(1-\mu^2)^{1/2}v$, and $\omega=dp/dt$.

The two-layer model is schematically summarized in figure 6. The lower troposhere is represented by the fields at 750 mb and the upper troposphere by those at 250 mb. The real tropical atmosphere, on the other hand, is more complicated than this as can be seen from figure 1. For example, the flow at 200 mb is not representative of the upper troposphere. Thus, rather than thinking of the results of the model as representative of a particular level in the atmosphere, they should more correctly be thought of as representing the average conditions of the layer.

At the upper boundary, we set $\omega=0$, while at the earth's surface, we assume that $\omega=\omega_G(\mu, \varphi)$, a known function. The subscript G infers that the quantity is evaluated at the lower boundary. We also assume that a quantity evaluated at the interface of the two layers is the mean of the quantities evaluated at levels 5 and 2. That is,

$$\chi_{p=1/2}=\frac{\chi_1+\chi_2}{2} \tag{23}$$

where the subscript denotes the level to which the variable applies. Then, using the upper and lower boundary conditions, we may approximate the vertical advection terms by

$$\omega\left.\frac{\partial\Delta}{\partial p}\right|_1=\omega(\Delta_2-\Delta_1)$$

and

$$\omega\left.\frac{\partial\Delta}{\partial p}\right|_2=2\omega_G(\Delta_G-\Delta_2)+\omega(\Delta_2-\Delta_1) \tag{24}$$

where $\Delta_G=\Delta(p=1)$.

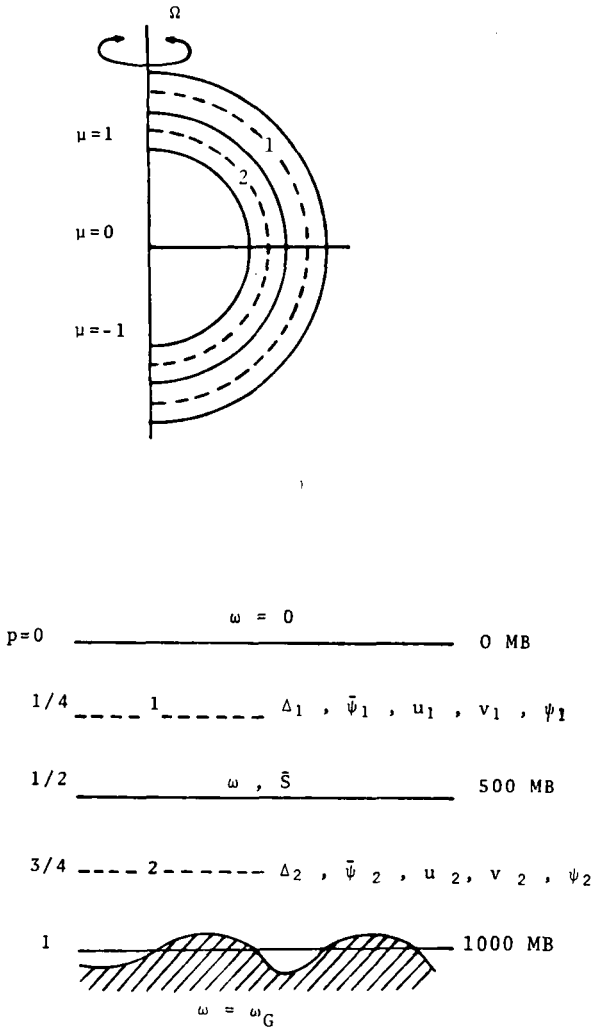

FIGURE 6.—The two-layer model.

We will assume the following simple linear dissipation laws (Charney 1959):

$$\mathbf{F}_1(\mu,\varphi)=-K_2(\mathbf{V}_1-\mathbf{V}_2)(1-\mu^2)^{1/2},$$

and

$$\mathbf{F}_2(\mu,\varphi)=[K_2(\mathbf{V}_1-\mathbf{V}_2)-K_1\mathbf{V}_2](1-\mu^2)^{1/2}, \qquad (25)$$

$$\dot{Q}(\mu,\varphi)=\mathcal{Q}(\mu,\varphi)+K_3(\psi_2-\psi_1).$$

Here, K_1, K_2, and K_3 are representative of a surface drag coefficient, a coefficient of small-scale exchange of horizontal momentum vertically between the layers of the model, and a radiational cooling coefficient, respectively. $\mathcal{Q}(\mu, \varphi)$ is the known heating function. The values we will use in all our calculations are $K_1=0.0308$, $K_2=0.00343$, and $K_3=0.00206$ (Charney 1959). The value of ω_G is determined by using the approximate condition that

$$\omega_G=-\Delta_G\frac{\partial}{\partial\varphi}h(\mu,\varphi) \qquad (26)$$

where $h(\mu,\varphi)$ is the nondimensional orography function defined by

$$h(\mu,\varphi)=\frac{gh'(\mu,\varphi)}{R\bar{T}(p=1)}.$$

The longitudinal dependency is separated out by expanding the variables in Fourier series as in eq (7). The appropriate form of eq (22) is reached in the following manner. The momentum and continuity equations are expressed at levels 1 and 2, and the thermodynamic equation is given for the interface ($p=½$). After using the continuity equation to eliminate ω and with eq (24), (25), and (7), we finally arrive at a set of equations in the μ-dependent complex Fourier coefficients. These are

$$[s(B+2C)-iK_2]U_1^s-i[CD-A_1\mu+D(B+C)]V_1^s+iK_2U_2^s=-s\Psi_1^s,$$

$$A_1\mu U_1^s+i[s(B+C)-iK_2]V_1^s-K_2V_2^s=-D(\Psi_1^s),$$

$$iK_2U_1^s+i[CD+A_2\mu-D(B+C)]V_2^s+(sB-iK_1)U_2^s=-s\Psi_2^s-F_1^s(\mu),$$

$$A_2\mu U_2^s-K_2V_1^s+i[s(B-2C)-iK_2]V_2^s=-D(\Psi_2^s),$$

$$sU_1^s+sU_2^s-iD(V_1^s)-iD(V_2^s)=F_2^s(\mu), \qquad (27)$$

and

$$\frac{s\bar{S}}{(1-\mu^2)}U_1^s-i\left[\frac{\bar{S}}{1-\mu^2}D-C(1+2B)\mu\right]V_1^s+iC(1+2B)\mu V_2^s=(sB-iK_3)(\Psi_2^s-\Psi_1^s)+iF_3^s(\mu)$$

where $B=(\Delta_1+\Delta_2)/2$, $C=(\Delta_1-\Delta_2)/2$, and $A_j=2\Delta_j+1$ where $j=1, 2$. B and C represent the barotropic and baroclinic parts of the basic zonal flow, respectively.

The forcing functions, $F_i^s(\mu)$, are defined by

$$F_1^s(\mu)=-is(1-\mu^2)\Delta_G(\Delta_1+\Delta_2-2\Delta_G)h^s(\mu),$$

$$F_2^s(\mu)=2is(1-\mu^2)\Delta_G h^s(\mu),$$

and

$$F_3^s(\mu)=-\mathcal{Q}^s(\mu). \qquad (28)$$

For simplicity of notation, the s superscript will henceforth be understood.

Numerical Method

The numerical procedure used to solve eq (27) is similar to that used by Mak (1969). Rather than following the usual procedure of first reducing the set of equations to the simplest possible form, we initially expanded eq (27) in finite-difference form and then reduced. This precludes the problem of handling very complicated operators resulting from the μ-dependent coefficients. The finite-difference scheme chosen is a one-dimensional version of the "staggered centered-difference" scheme described by Phillips (1962). The resulting six first-order difference equations are reduced to two linear, complex, second-order, coupled difference equations by a relatively straightforward procedure.

Following the procedure outlined in appendix 3, we derive two linear, complex, second-order, coupled difference equations. These are

$$p_1^kV_1^{k+1}+p_2^kV_1^k+p_3^kV_1^{k-1}+p_4^kV_2^{k+1}+p_5^kV_2^k+p_6^kV_2^{k-1}=r_1^k+r_2^k+r_3^k+r_4^k+r_5^k+r_6^k$$

and

$$q_1^kV_1^{k+1}+q_2^kV_1^k+q_3^kV_1^{k-1}+q_4^kV_2^{k+1}+q_5^kV_2^k+q_6^kV_2^{k-1}=t_1^k+t_2^k+t_3^k+t_4^k+t_5^k+t_6^k \qquad (29)$$

where p_j^k and q_j^k are complex coefficients and r_j^k and t_j^k are the complex nonhomogeneous coefficients. The coefficients have the following functional form:

$$p_j^k,\ q_j^k = fn(\mu, s, \bar{S}, B, C, K_1, K_2, K_3, F_1, F_2, F_3)$$

and

$$r_j^k,\ t_j^k = fn(\mu, s, \bar{S}, B, C, K_1, K_2, K_3, F_1, F_2, F_3).$$

Equations (29) are separated into real and imaginary parts providing a set of four real, coupled difference equations.

To cover the latitude zone between the two poles, we used 41 gridpoints ($k=1$, 41 with $\Delta\mu=0.05$). The advantage of the cosine of colatitude as the latitudinal coordinate is here apparent since half the gridpoints in the μ-space (-1, 1) lie between $\pm 30°$. Expressing the set of real difference equations at each point in the range, we arrive at a system of 4×39 (156) linear simultaneous equations in 164 unknowns. The balance of the unknowns is provided by the boundary conditions at the poles, which are

$$V_1^{k=1} = V_1^{k=41} = 0$$

and (30)

$$V_2^{k=1} = V_2^{k=41} = 0.$$

The system of equations may be expressed in the matrix form

$$\mathbf{A}*\mathbf{X}=\mathbf{F} \tag{31}$$

where $\mathbf{A}(p_j^k, q_j^k)$ is the 156×156 coefficient matrix $\mathbf{X}(V_1^k, V_2^k)$ is the 1×156 variable matrix, and $\mathbf{F}(r_j^k, t_j^k)$, is the 1×156 nonhomogeneous matrix. Fortunately, the matrix is banded (i.e., consists of a main diagonal and seven adjacent upper and seven adjacent lower diagonals, while the remainder of the terms are zero), allowing the use of a fast numerical "Gauss elimination" method (International Business Machines 1968) to invert eq (31).

The Basic Fields

The basic zonal wind fields were obtained from Vincent (1969) and are shown in figure 7. Three basic fields are used. The first two are the seasonal averages for DJF and JJA. The most apparent features are the large horizontal and vertical shears within the Tropics. For example, in the winter hemisphere of DJF and JJA, large shears exist at quite low latitudes.

The third field, an idealized approximation of the annual mean wind field (labeled ANN), is given by the expressions

$$\bar{U}_1(\mu) = 18 \sin \frac{3\pi}{2}(\mu+1) + 14(1-\mu^2)$$

and (32)

$$\bar{U}_2(\mu) = 7 \sin \frac{3\pi}{2}(\mu+1) + 2(1-\mu^2).$$

ANN will be used to consider the response of the system to hypothetical forcing functions.

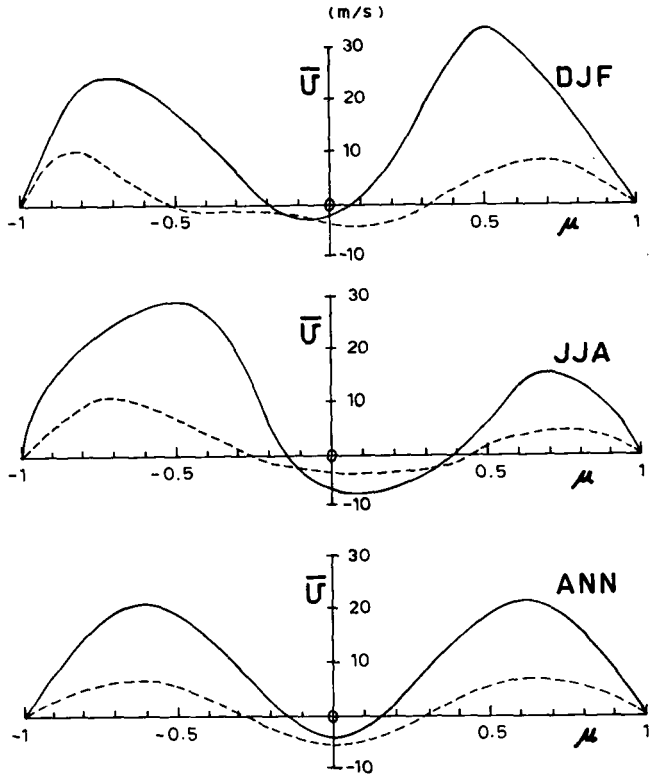

FIGURE 7.—The three basic zonal wind distributions (m/s) for DJF, JJA [from Vincent (1969)], and the symmetric annual field, ANN. The curves represent $\bar{U}$ at 250 (solid) and at 750 mb (dashed)

We found two possible distributions of the basic zonal velocity at $p=1$ for the model. The first, a linear extrapolation of the basic wind field to the ground, produces very strong easterlies at $p=1$ in regions of strong shear in midlatitudes (e.g., at $\mu=0.5$ in DJF). In better agreement with the observations is the assumption that

$$\bar{U}_{p=1}(\mu) = \tfrac{1}{2}U_2(\mu). \tag{33}$$

For the static stability, we found that $\bar{S}=0.0083$ best represents the annual mean static stability at 500 mb between $\pm 30°$ of latitude. This value is approximately the same as that used by Mak (1969).

5. RESPONSE OF THE TWO-LAYER MODEL

In an attempt to approach an understanding of the manner in which a basic state containing both horizontal and vertical shear will react to the complicated forcing fields, we will consider some illustrative examples. Specifically, we will consider the reaction of the hypothetical symmetric basic state ANN to the placement of the idealized energy sources at specific locations. Following this, we will consider the response of the DJF and JJA basic fields to the combination of thermal and orographic forcing, and finally we will compare the predicted motions with some observed values.

It is interesting at this point to anticipate what may be the important physical processes governing the

response of the model in low latitudes. During the description of the model, we discussed the incorporation of dissipative mechanisms. The values chosen for the effects of surface friction, the small-scale exchange of horizontal momentum, and radiational cooling provide decay times of approximately 6, 25, and 40 days, respectively. Near the Equator, the magnitude of the basic current is about 5 m/s. This provides an advective time scale (defined in our model as the time required for a parcel to be advected by the basic current over one longitudinal wavelength) for the longest longitudinal scale ($s=1$) on the order of 80 days. For $s=2$, the time scale reduces to 40 days, and so on. By comparing the dissipative time constants with the advective time scales, we can expect that the dissipative effects will be very important for equatorial motions. As we move into the westerlies, the advective time scale will be much smaller because of the increase in magnitude of the basic current and decrease in the circumference of the earth. Consequently, frictional effects will be less dominant.

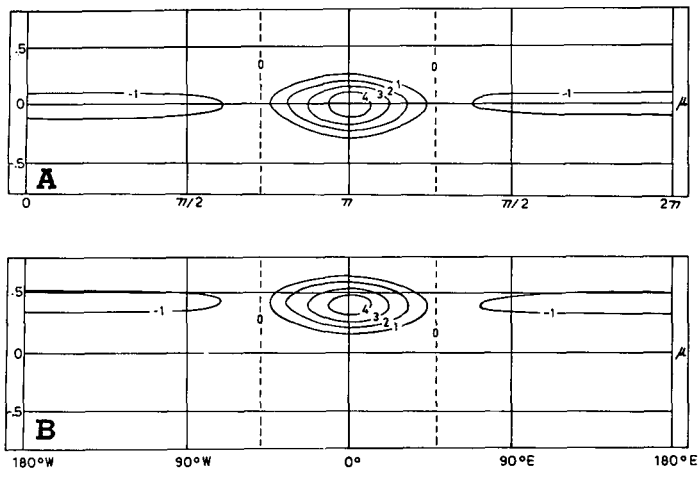

FIGURE 8.—Distribution of heating (10^2 cal·cm^{-2}·day^{-1}) or orography (km) for (A) $\mu_c=0$ and (B) $\mu_c=0.4$ for the hypothetical forcing fields given by eq (34).

Response to Idealized Forcing

The basic field, ANN, will be forced by a distribution of heating or orography of the form

$$F(\mu, \varphi)=A \exp\left[\frac{-81(\varphi-\pi)^2}{4\pi^2}-25(\mu-\mu_c)^2\right] \qquad (34)$$

to provide a function that is symmetric about the prime meridian and some latitude $\mu=\mu_c$ and e-folds within $\pm 40°$ of longitude and $\pm 12°$ of latitude. For a heating function, we chose $A=600$ cal·cm^{-2}· day^{-1}, while for the orographic case, we let $A=6000$ m. The amplitudes of the function were chosen to correspond to the amplitudes of the heating over India in JJA and the Himalayan Mountains, respectively. Figure 8 shows a recomposition of the Fourier expansion of eq (34) with $\mu_c=0$ and 0.4, using the first nine nonzero Fourier coefficients.

Response with $\mu_c=0$. Figure 9 shows the perturbation horizontal velocity and height fields due to the hypothetical heat source centered at $\mu=0$ and $\varphi=\pi$. The effect of a similarly located orographic function is shown in figure 10.

We will consider the heating function first. Both velocity fields (250, 750 mb) are characterized by strong

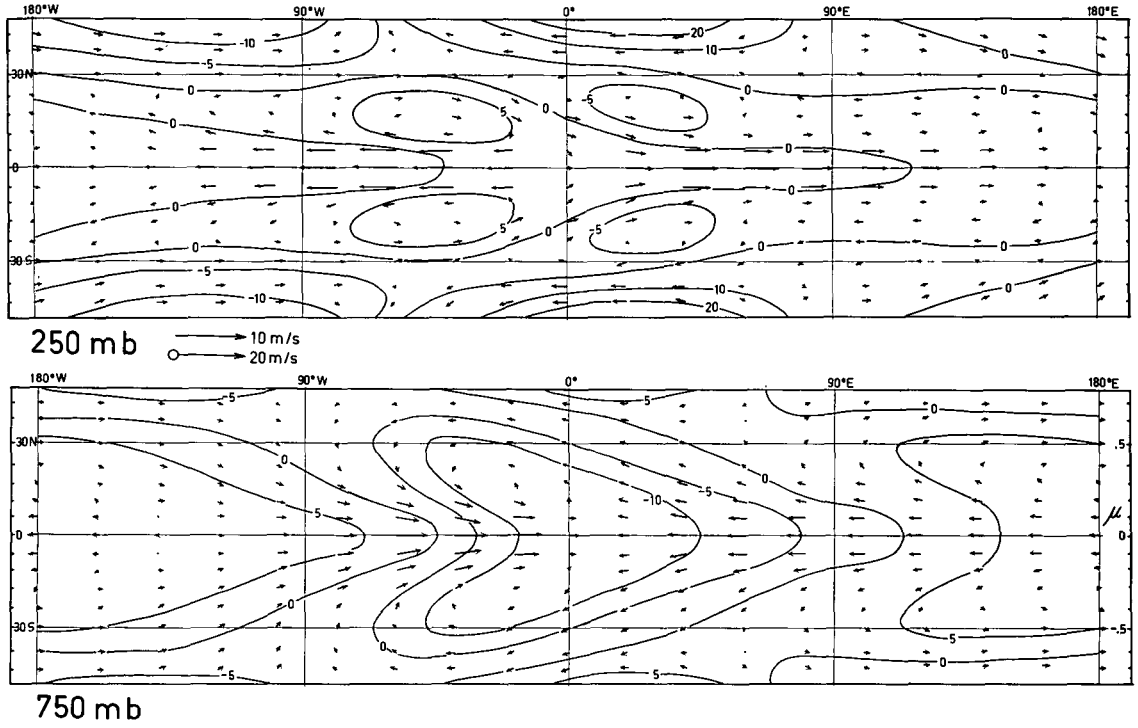

FIGURE 9.—Horizontal perturbation velocity (vectors) and geopotential height deviations (solid lines) of the basic field, ANN, at 250 and 750 mb in response to an isolated heat source given by eq (34) with $\mu_c=0$ and $A=600$ cal·cm^{-2}·day^{-1}. The vector magnitude is proportional to the indicated scale and the geopotential heights are in meters.

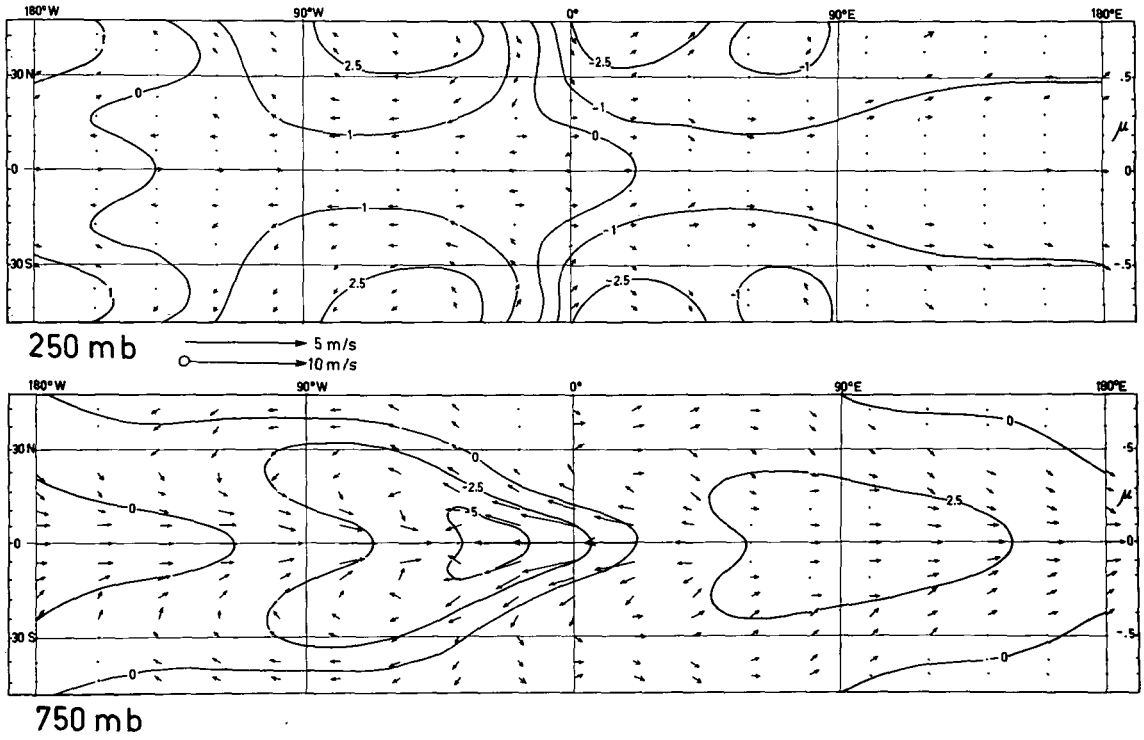

FIGURE 10.—Same as figure 9 for orographic forcing given by eq (34) with $\mu_c=0$ and $A=6000$ m. Note that the vector magnitude scale has been increased by a factor of four.

zonal currents located along the Equator flowing into the heat source region at 750 mb and out of it at 250 mb. Subsidence in the heat sink region with upper level convergence and lower level divergence completes the zonal circulation. Away from the Equator, the motions are characterized by weak cyclonic and anticyclonic circulations that completely change phase between the two levels.

The narrow zonal perturbation velocity maximum along the Equator is most likely the response of the rotationally trapped Kelvin wave mentioned earlier. From the height field we see that these motions are nearly completely ageostrophic, with the wind blowing down the pressure gradient, inferring that the flow is most likely a balance between the impressed pressure field due to the heating and the frictional dissipation. Toward higher latitudes, the height contours become nearly parallel to the flow, indicating the increasing importance of rotation.

Turning our attention to the orographic forcing, we see that the basic field appears to react in a completely different manner than to the similarly located heating. Note especially that the lower boundary forcing appears to have little influence on the upper layer. (The magnitudes of the horizontal velocity vectors have been doubled in fig. 10 so as to exaggerate their relative smallness.)

In the simplified continuous model, we found that the response of the Kelvin wave to orographic forcing possesses very large amplitudes and was oscillatory in its vertical structure, which is contrary to the equatorial response here. The difference appears to lie with the effect of dissipative processes. To illustrate this, we will consider the effect of dissipation in the continuous model. The vertical wave number, m, of the Kelvin wave is given by eq (16), which together with eq (50), may be written as

$$m^2 \approx \frac{s^2 \overline{S}(Z)}{\lambda_s^2}.$$

The effect of a simple linear dissipation process (e.g., dissipation proportional to $K\mathbf{V}$ where K is a frictional coefficient) could have been included by redefining the Doppler-shifted frequency, λ_s, in eq (44a) and (44b) to be

$$\lambda_s = -\left(\frac{\delta s}{2} + iK\right),$$

so that, by using eq (16) and (50), we now get

$$m^2 = \frac{s^2 \overline{S}(Z)}{\left(\frac{\delta s}{2} + iK\right)^2}. \tag{35}$$

Since the advective time scale of the near-equatorial motions is small compared with the frictional time constant, it follows that $\delta s/2 \ll K$ so that $m^2 < 0$. Alternatively, we may say that the Doppler-shifted period is very large compared with frictional time scale. Thus, from eq (19), we see that the solutions decay with height. Following this further, we find that, if we express the continuity equation at the lower level and use eq (24), we obtain

$$2(1-\mu^2)(\omega-\omega_G) = \nabla \cdot \mathbf{V}_2. \tag{36}$$

If the amplitude of the Kelvin wave decreases exponentially with height, then $\omega \ll \omega_G$. Using eq (26), we find that

$$\nabla \cdot \mathbf{V}_2 \approx -\Delta_G \frac{\partial}{\partial \varphi}[h(\varphi,\mu)]. \tag{37}$$

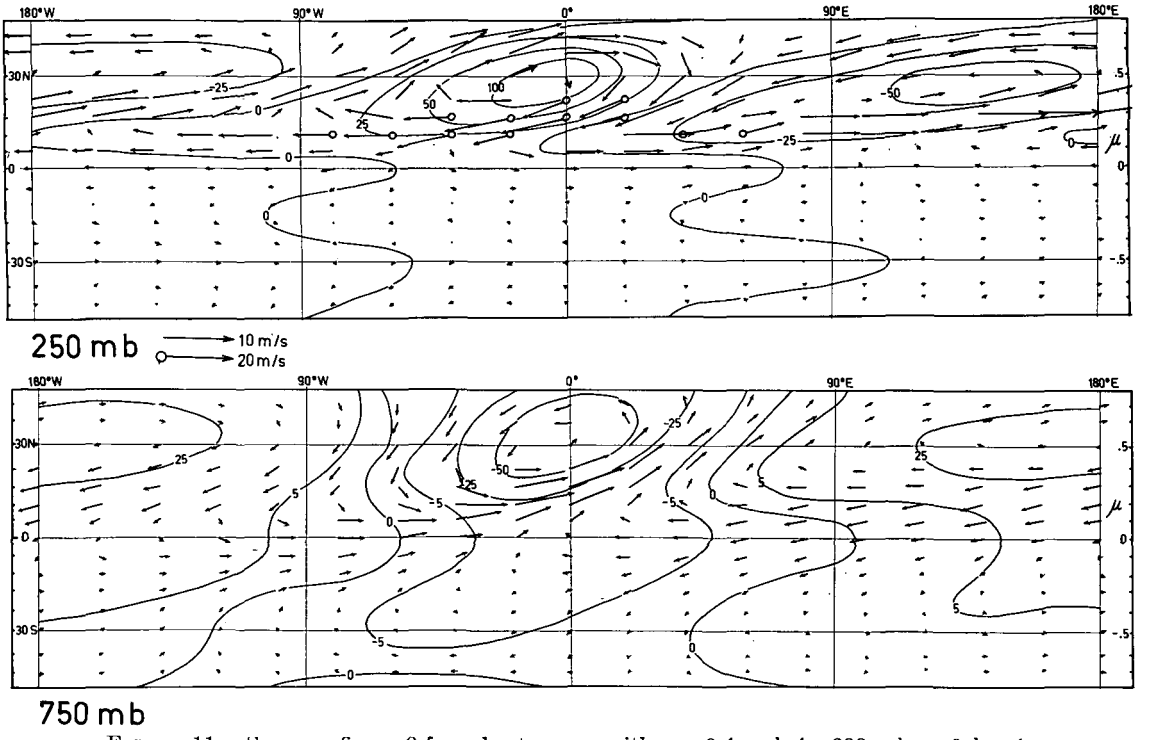

FIGURE 11.—Same as figure 9 for a heat source with $\mu_c=0.4$ and $A=600$ cal·cm^{-2}·day^{-1}.

Thus, near the Equator, the divergence field is almost completely determined by the distribution of orography. For $\Delta_G<0$, eq (37) provides divergence to the east of the mountain and convergence to the west, features that are observed in figure 10.

Finally, we should ask why a strong response occurs in the upper layer of the model with thermal forcing but not with orographic forcing. Primarily, this is due to the manner in which the forcing enters the model. Orographic forcing enters the model at the lower boundary in the regions of maximum dissipation. Heating, on the other hand, enters the equations as a nonhomogeneous term in the thermodynamic equation, which is expressed at the midlevel. Thus, in this model, both layers are driven directly at the interface in a region of less dissipation.

Response with $\mu_c=0.4$. Figures 11 and 12 show the perturbation horizontal velocity fields due to the thermal and orographic forcing, respectively. Considering first the thermal response, we note that the magnitudes are much larger than they were for $\mu_c=0$. This is to be expected because of the increased effect of the rotation of the earth at the higher latitudes plus the fact that the phase speeds of the free Rossby waves in the westerlies are sufficiently slow to allow them to approach a quasi-resonant response.

The fields are characterized by strong cyclonic (anticyclonic) circulations in the lower (upper) region in the vicinity of the heat source, and elongated reverse circulations are associated with the cooling region. Relative high and low height anomalies are associated with the anticyclones and cyclones, respectively.

Especially evident is the asymmetry of the circulation; centers tend to lean steeply from the southwest to the northeast. The maximum wind speeds are so arranged as to transport momentum poleward. The Southern Hemisphere appears to be only slightly affected by the heating at $\mu_c=0.4$, although at 750 mb, there is some cross-equatorial flow. The cross-equatorial flow is small, however, compared with the meridional motions to the north.

There is also evidence of a change in form of the response close to the latitude where the basic wind field changes sign (i.e., at the critical latitude of the steady motions). This is most apparent in the 250-mb motions where the flow becomes nearly zonal and down the geopotential height gradient. Possibly the Kelvin wave associated with the equatorial easterlies is being excited by a southerly energy flux.

The response of the orography function is vastly different from that of the $\mu_c=0$ case in both form and magnitude. East of the mountain (leeward), a series of oscillations has developed that progressively decreases in amplitude to the east. The most intense features are the ridge and trough immediately upstream and downstream of the mountain. All features appear to slope slightly upwind in the vertical. Also, the magnitude of the response is at least an order of magnitude larger in the upper level than it was when the hypothetical mountain was placed at the Equator.

The orographic feature appears to exert little influence upon the Southern Hemisphere. We do note, however, that at 250 mb the velocities near the Equator are fairly large. Evidently, the upper troposphere at very low latitudes is more influenced by this "remote" forcing than by the orographic forcing at the Equator itself. One can envisage the situation where, with orographic forcing at, say, $\mu=0$ and 0.4, the upper and lower levels would show little coherence about the Equator.

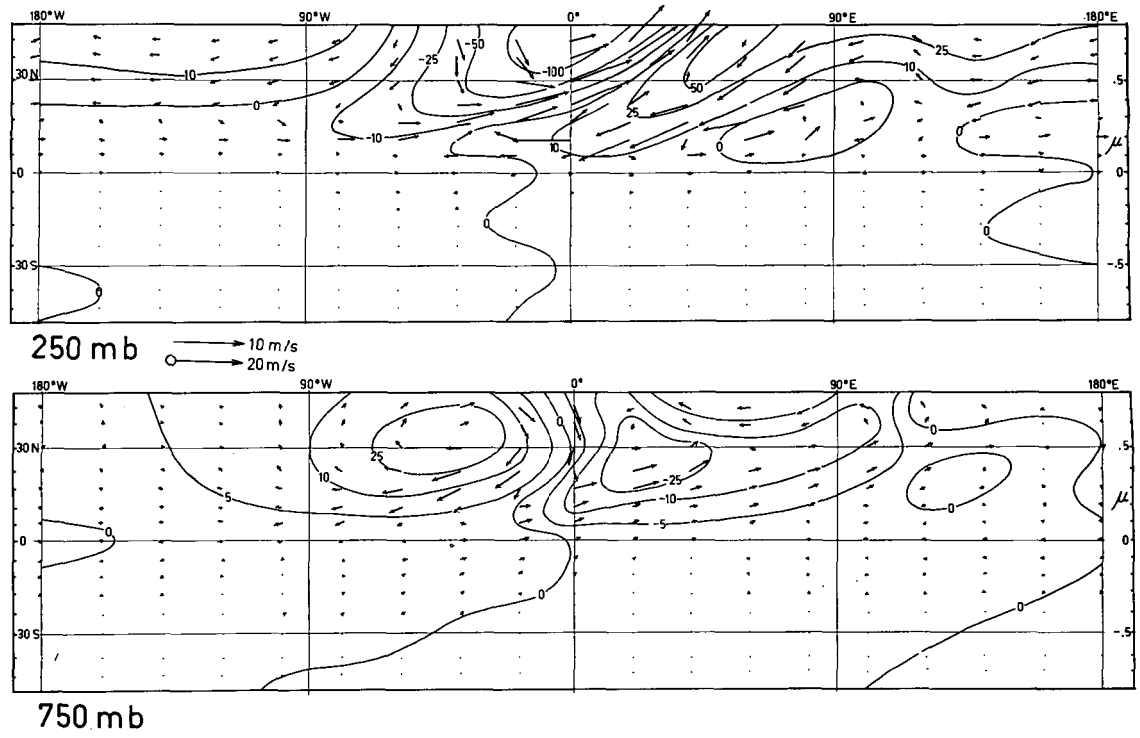

FIGURE 12.—Same as figure 9 for orographic forcing with $\mu_c=0.4$ and $A=6000$ m.

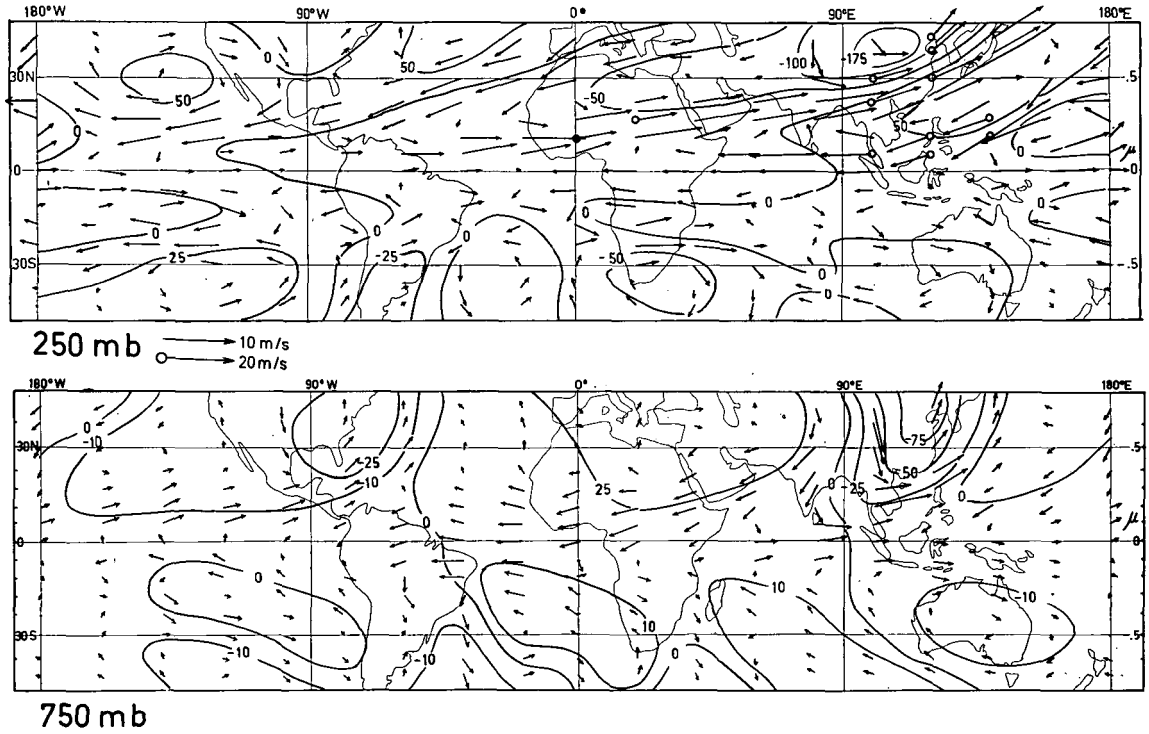

FIGURE 13.—Same as figure 9 for the response of the DJF basic field to the combined orographic and DJF latent-heat forcing fields shown in figures 2A and 2B, respectively.

Response to Seasonal Forcing

The seasonal forcing functions were compiled from a combination of the orography and seasonal thermal forcing fields discussed in section 2. The perturbation velocity responses of the two basic states, DJF and JJA, are shown in figures 13 and 15. Comparisons are made with data originating from long-term mean values of the tropical atmosphere compiled by Kidson et al. (1969) and Newell et al. (1972). The observed perturbation velocity fields are shown in figures 14 and 16. More recently, Krishnamurti (1970) studied the mean structure of the 1967 JJA field using, in addition to conventional data, wind observations from aircraft. Considering the large differences in the lengths of the data records, we find few differences between the results of the two studies.

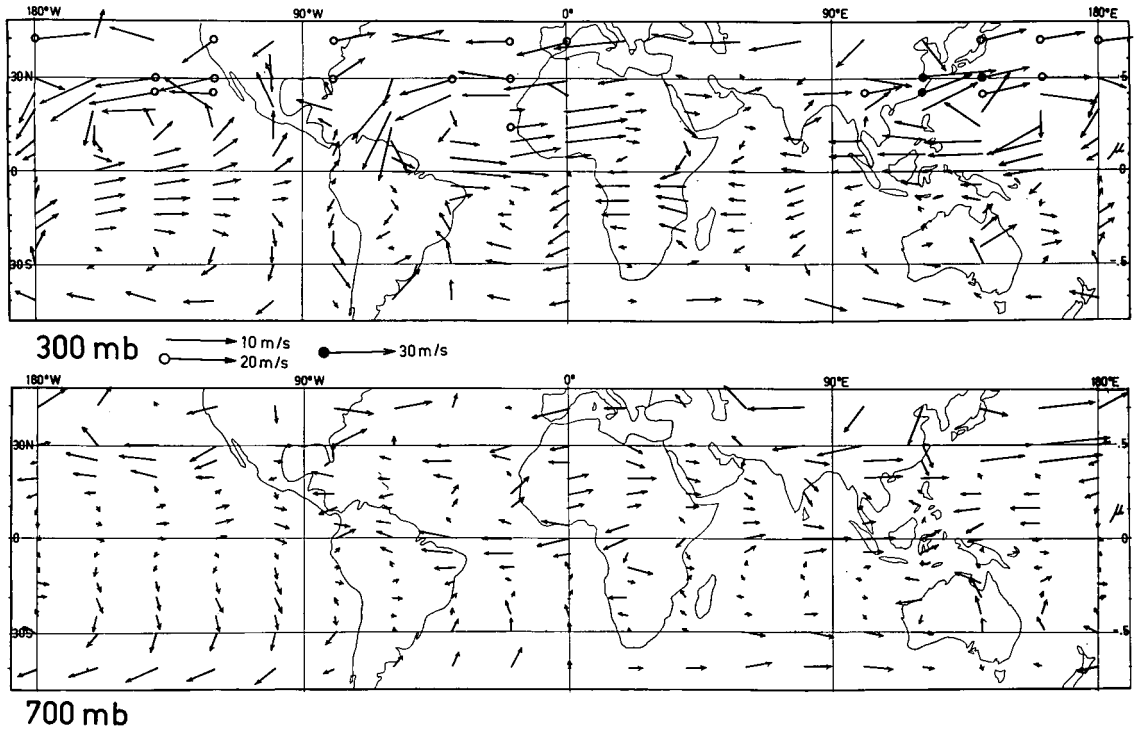

FIGURE 14.—Observed horizontal perturbation velocity field for DJF. Data from Newell et al. (1972).

When comparing the computed and observed fields of motion, one should bear in mind the basic aim of the study. That is, to determine what role the various forcing functions situated within the Tropics play in the maintenance of the steady-state structure of the tropical atmosphere. Thus, if we assume that the model is capable of at least handling the gross features of the stationary flow, both the similarities and differences between the observed and computed fields of motion are of equal importance in approaching this aim.

Comparison of the DJF results. In general, the correspondence between the observed and computed fields appears to be a function of latitude (figs. 13, 14). At low latitudes, the agreement is fair, but it decreases to poor as we progress poleward into the extratropical latitudes. The reasons behind the similarities and differences will be discussed later.

In the Atlantic Ocean region, the low-level computed and observed fields show strong easterly flow along the Equator extending from equatorial Africa to the trough system centered in the Amazon River Valley. Aloft, the strong westerlies associated with the upper level trough extending from the Middle East to Central America are predicted quite well in both magnitude and position. The magnitude of the easterlies to the north are underestimated, however.

Some similarity exists between the observed and predicted fields at very low latitudes in the Pacific Ocean. To the north, the agreement is especially poor; the low-level anticyclone observed at 30°N is not predicted and the band of easterlies in the upper troposphere is observed north of its computed position. In the South Pacific, the predicted motions are somewhat more complicated than those observed, although the simplicity of the latter field could be due to the lack of observations. However, both low-level fields show an elongated anticyclone and an east–west oriented trough to the south.

In the Eastern Hemisphere, most of the upper level low-latitude and northern hemispheric flow is predicted. Most apparent is the strong ridge stretching from east of Asia to Africa, with the associated easterly maximum over Indonesia and westerlies over Africa, although the model tends to overestimate the westerlies over Arabia. The position of the Himalayan lee trough appears to coincide with its observed position, although there are some differences poleward of 30°N and east of Japan. South of the Equator, the prediction of the flow over South Africa is poor with the westerlies overestimated and displaced too far north. Over northwestern Australia and the eastern Indian Ocean, there is some similarity between the two flow fields.

In the lower layer, the model predicts a large cyclonic flow converging into a westerly maximum along the Equator into Indonesia, a northeasterly flow over India, and a trough over China. In addition to these similarities with the observed flow, a large difference occurs over the northern Sahara Desert and northwestern Indian Ocean north of where the model predicts easterlies instead of westerlies.

Comparison of the JJA results. Both the computed and observed Northern Hemisphere flow fields (figs. 15, 16) are dominated by two major circulation systems, a large cyclonic circulation over southern Asia with a trough extending from the China Sea to central Africa and a

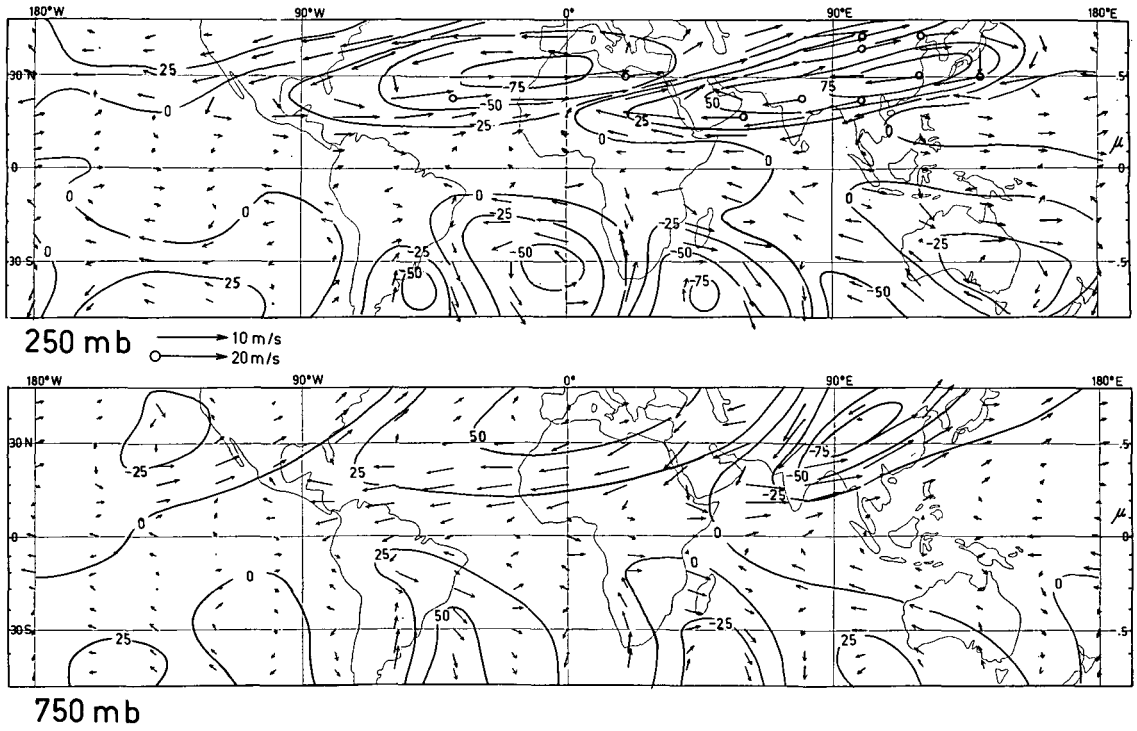

FIGURE 15.—Same as figure 9 for the response of the JJA basic field to the combined orographic and JJA latent-heat forcing fields shown in figures 2A and 2C, respectively.

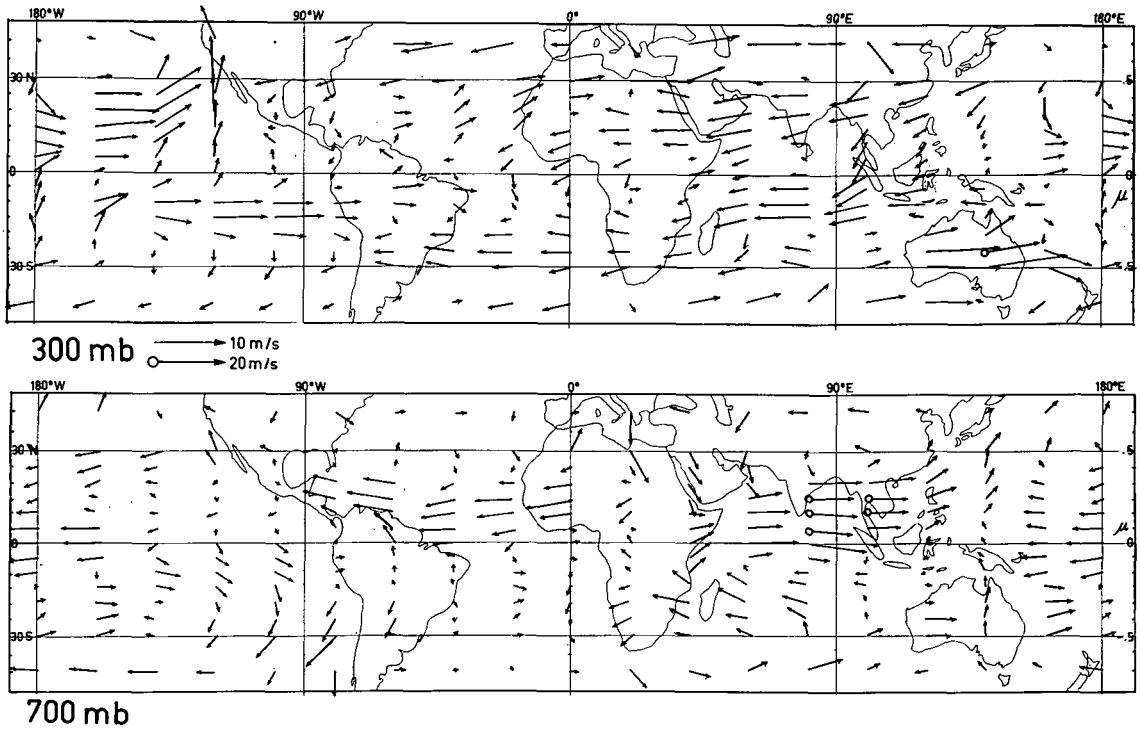

FIGURE 16.—Same as figure 14 for JJA.

large anticyclone and ridge system that dominates the Atlantic region. However, the model once again fails to predict the flow over the North Pacific Ocean.

At 750 mb, the model predicts the strong Indian cyclonic circulation, the band of strong westerlies extending across the Indian Ocean from Africa to the North China Sea, and the converging flow into this velocity maxima from the Southern Hemisphere. However, the magnitude of the flow just to the east of India is underestimated by nearly a factor of two.

The low-level flow over the Sahara Desert and West Africa is reproduced fairly well, but in South Africa the prediction is poor. In the predicted field, the Indian Ocean anticyclone is displaced to the east of its observed position.

It is evident from the discussion of the response of the two-layer model that, in certain regions of the tropical

atmosphere, other factors not included in the model must be of importance. This is most noticeable at the northern and southern extremities of the Tropics. On the other hand, the similarity of the flow at very low latitudes indicates that local forcing is also important. We will discuss the relative importance of these mechanisms in the next section.

6. ENERGETICS OF THE TWO-LAYER MODEL

The Energy Equations

The eddy kinetic energy, KE, equation is readily obtained by multiplying eq (22a) by u and eq (22b) by v and adding the resultant equations. Multiplying eq (22d) by $(\partial\psi/\partial p)/\bar{S}$ yields the eddy available potential energy, AE, equation. By first expressing the KE and AE equations in the two-level system, then nondimensionalizing and integrating over the longitude domain, we obtain, respectively, the zonally averaged eddy kinetic energy and available potential energy equations. These are

$$(\Delta_1-\Delta_2)[\omega(u_1+u_2)+\omega_G u_2]-\left(\frac{d\Delta_1}{d\mu}[u_1v_1]+\frac{d\Delta_2}{d\mu}[u_2v_2]\right)$$
$$-\frac{d}{d\mu}([v_1\psi_1]+[v_2\psi_2])-2[\omega(\psi_1-\psi_2)]+\frac{2}{1-\mu^2}\{K_2([u_1u_2]$$
$$+[v_1v_2])-(K_2[\mathcal{K}_1+\mathcal{K}_2])\}=[\psi_2\omega_G] \quad (38)$$

and

$$\frac{(\Delta_1\Delta_2)(1+\Delta_1+\Delta_2)\mu[(v_1+v_2)(\psi_1-\psi_2)]}{2\bar{S}}$$
$$+2[\omega(\psi_1-\psi_2)]-K_3[A]=[(\psi_1-\psi_2)\mathcal{Q}(\mu,\varphi)] \quad (39)$$

where

$$[\ \ ]=2\pi^{-1}\int_0^{2\pi}d\varphi$$

in these two equations *only*, and

$$\mathcal{K}_i=\frac{(u_i^2+v_i^2)}{2} \qquad (i=1,2)$$

and

$$A=\frac{(\psi_1-\psi_2)^2}{2\bar{S}}.$$

Each term in eq (38) and (39) refers to a specific physical process. The first two terms of eq (38) represent the conversion of kinetic energy of the mean zonal flow, KZ, to KE by vertical and horizontal Reynold stresses, respectively [symbolically referred to as (KZ·KE)]. The third term represents the redistribution of KE by the convergence of wave energy flux, sometimes referred to as the pressure work term, PW. PW only redistributes KE and integrates to zero over the whole atmosphere; therefore, it may be thought of, at a particular point, as a *local* KE source due to *remote* forcing. The conversion between AE and KE, (AE·KE), is given by the next term. Since $(\psi_1-\psi_2)$ is proportional to the temperature of the midlevel of the model, a positive conversion depends upon the rising (sinking) of warm (cool) air. The fifth and sixth terms represent the destruction of KE by small-scale processes (D_{FRIC}). The sources of KE, S_{MT}, due to the orographic forcing are shown on the right-hand side of eq (38).

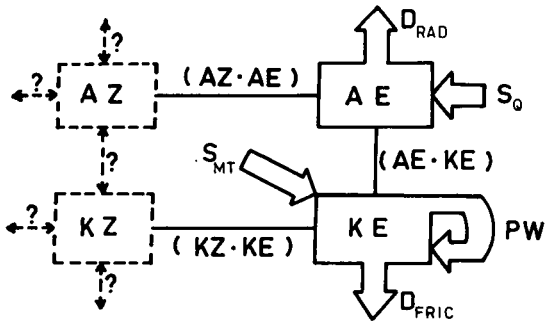

FIGURE 17.—Energetics of the model atmosphere.

The first term in the AE equation represents the conversion of zonal available potential energy, AZ to AE, (AZ·AE), and is positive when there is a poleward (equatorward) flux of warm (cold) air (i.e., if $\Delta_1>\Delta_2$ so that $\bar{T}$ decreases poleward). The (AE·KE) conversion is given next and links the AE and KE equations. The third member of eq (39) represents the parameterized destruction of AE by radiative and small-scale processes, D_{RAD}, while the final term is the source of AE due to thermal forcing, S_Q. S_Q is positive when the system is heated where it is warm or cooled where it is cold.

In the notation introduced in the preceding paragraphs, the two zonally averaged energy equations may be written in the following manner:

$$(KZ\cdot KE)+(AE\cdot KE)+PW+D_{FRIC}=S_{MT} \quad (40)$$

and

$$(AZ\cdot AE)+(KE\cdot AE)+D_{RAD}=S_Q \quad (41)$$

where D_{FRIC} and D_{RAD} are negative by definition.

The energetics of our model is schematically presented in figure 17. Since the energetics of the basic state is not described, the energetics of the model must be considered incomplete. In the remainder of this section, we will discuss the energetics of the linear response of the two-layer model due to forcing by both the hypothetical and seasonal forcing fields and briefly compare the latter results with some observed values and with those computed by Manabe et al. (1970).

Energetics of the Hypothetical Cases

Energetics with $\mu_c=0$. Figures 18 and 19 portray graphically the AE and KE balances that were expressed mathematically in eq (38) and (39). Each process is shown as a function of latitude and identified with the notation used in eq (40) and (41).

Considering the thermal case first, we find that the source term has a maximum at the Equator and decays fairly rapidly towards the poles. Except for a small radiational dissipation, the increase in AE is nearly balanced by the creation of KE. The KE is then distributed latitudinally by the pressure work effect. The positive values of PW near the Equator signify an equatorial flux of wave energy from both hemispheres.

469-748 O - 72 - 3

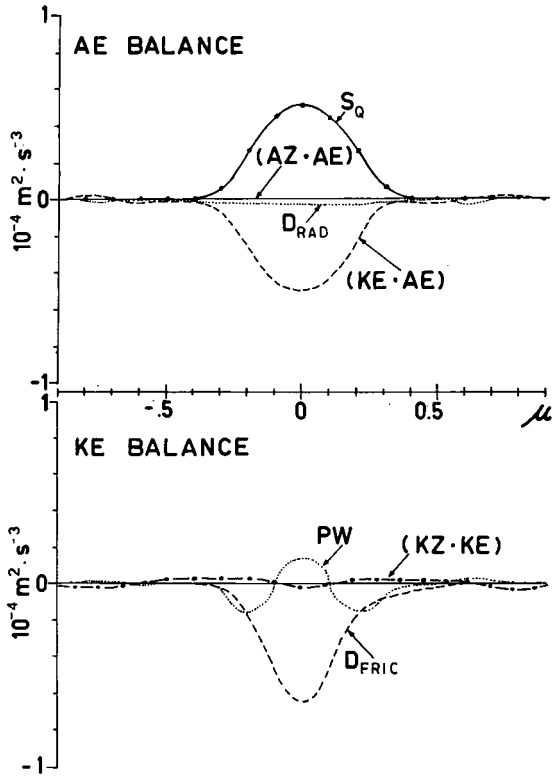

FIGURE 18.—Energy balance of the two-layer model with the basic state, ANN, due to forcing from the hypothetical heat source given by eq (34), with $\mu_c=0$ and $A=600$ cal·cm^{-2}·day^{-1}. For clarity, the (AE·KE) curve is shown only with the AE balance. The latitudinal coordinate is μ, the sine of latitude.

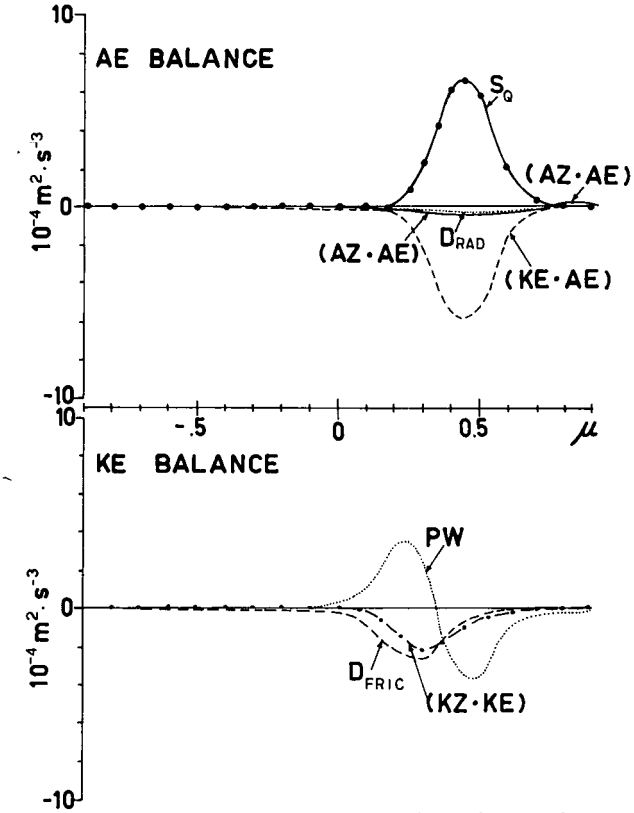

FIGURE 20.—Same as figure 18 for the hypothetical heat source given by eq (34) with $\mu_c=0.4$ and $A=600$ cal·cm^{-2}·day^{-1}. Note that the ordinate scale has been increased by an order of magnitude.

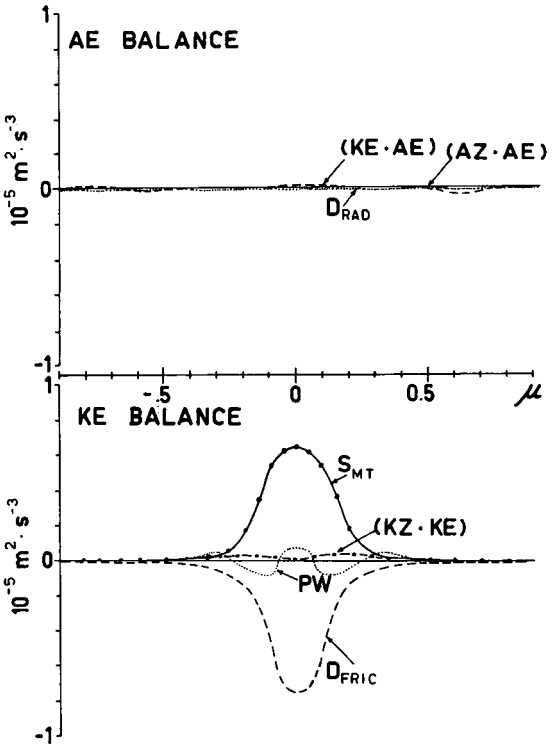

FIGURE 19.—Same as figure 18 for the hypothetical mountain given by eq (34) with $\mu_c=0$ and $A=6000$ m. Note that the ordinate scale has been decreased by an order of magnitude.

The flux reverses sign poleward of about $\mu=\pm 0.1$, which accounts for the small geostrophic motions in the subtropics observed in figure 9. Except for a small interchange between KZ and KE, the motions are effectively balanced by frictional dissipation.

The orographic forcing enters the system via the KE equation. The KE is redistributed both equatorward and poleward by the PW effect. There is almost zero conversion between KE and AE, probably a result of the constraints on the vertical velocity at the midlevel of the model by the exponentially decaying vertical structure of the Kelvin wave. The creation of KE is nearly completely balanced by dissipative processes.

Energetics with $\mu_c=0.4$. Figures 20 and 21 show, respectively, the energetics of the thermal and orographic forcing centered at $\mu_c=0.4$. The most striking feature is the order of magnitude increase in size of the response. This increased response is a result of the increased importance of rotation and the excitation of the quasi-resonant Rossby waves mentioned previously.

The distributions are also more complicated. In the thermally driven case, the AE is almost completely converted into KE. The small negative (AZ·AE) contribution is a result of the latitudinal advection of warm (cold) air into warm (cold) locations thereby causing the atmosphere to act like a weak refrigerator. The resulting KE is redistributed poleward and equatorward by the pressure work term. This produces a convergence of wave energy on the equatorial side of the heat source where, to maintain the KE balance, there is a large dissipation of KE through frictional processes and conversion to mean zonal kinetic energy. The latter con-

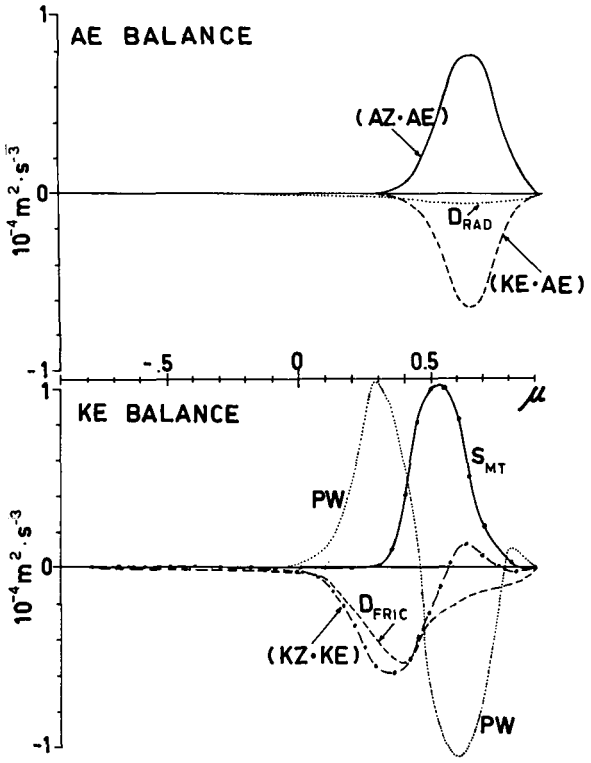

FIGURE 21.—Same as figure 18 for the hypothetical mountain given by eq (34) with $\mu_c=0.4$ and $A=6000$ m.

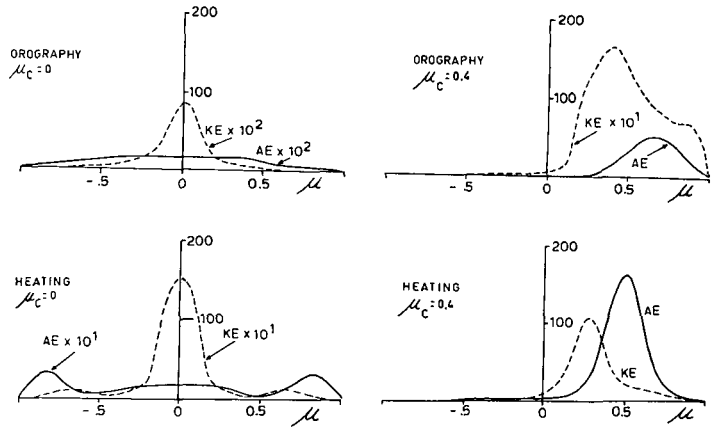

FIGURE 22.—Latitudinal distributions of AE and KE ($m^2 \cdot s^{-2}$) for the hypothetical orography given by eq (34) with $\mu_c=0$ and 0.4 and $A=6000$ m and for the hypothetical heating function with $\mu_c=0$ and 0.4 with $A=600$ cal·cm^{-2}·day^{-1}. Solid curves represent AE distributions and dashed lines represent KE.

version means that the steady perturbations are helping to maintain the basic zonal maxima. Note also that the role of frictional dissipation decreases away from the Equator as we anticipated earlier.

The kinetic energy balance in the orography case appears, at first glance, to be similar to the heating energetics. Both cases have the same PW structure and each converts KE into mean kinetic energy. The major difference is in the sign of the (AZ·AE) conversion, which is positive. This occurs because AE is increasing at the expense of the AZ on the poleward side of the mountain. Apparently, the mountain is causing latitudinal advection of warm air into cool regions and vice versa and thus is producing AE. As with the heating case, the role of frictional dissipation is seen to decrease as we move away from the Equator.

Distribution of AE and KE. Figure 22 shows the latitudinal distribution of AE and KE for the four hypothetical cases. The full and dashed curves represent the distributions of AE and KE, respectively. Both the heating and orography cases, with $\mu_c=0$, possess KE maxima about the Equator and comparatively small aggregates of AE. Even though small maxima exist in high latitudes for the heating case, the forcing centered at the Equator appears to yield only a small influence on the midlatitudes. With $\mu_c=0.4$, the AE and KE maxima have increased by an order of magnitude and have broadened their latitudinal extent of influence from low latitudes to the polar regions. We note also that, as we move poleward, the ratio AE/KE becomes progressively larger, a consequence of the increasing effect of rotation (Charney 1963).

The study of the energetics of these four modes suggests that the standing modes of the low latitudes are excited principally by two methods, either (1) by direct (AE·KE) conversion at low latitudes due principally to the latent heating or (2) by a pressure work redistribution of KE generated at higher latitudes by orographic and thermal forcing.

Computed Seasonal Energetics

The computed KE and AE balances for DJF and JJA are shown in figures 23 and 24, respectively. The common feature in each of the diagrams is the relative size of the energetics of the Northern Hemisphere compared with the Southern Hemisphere. This is probably due to the dominance of the Himalayan effect in DJF and the Indian heating in JJA. As we have noted previously, the effect of the forcing in the subtropics is seen to extend poleward in each hemisphere.

The features of the AE and KE balances are best explained by reference to the previous discussion of the hypothetical cases. We note especially that the model predicts a conversion of KE to zonal kinetic energy at all latitudes in the Tropics except for a narrow band about the Equator in both seasons. From Vincent's (1969) results, the computed sense of this conversion appears to agree with the observations for both tropical hemispheres in DJF and the Northern Hemisphere in JJA. For the latter season, observations (Kidson et al. 1969) indicate that in the Southern Hemisphere there is a strong northward flux of momentum between 5°N and 10°S above 200 mb. This results in a positive (KZ·KE) conversion, which is not predicted by our model. Since the main contribution to this conversion appears to come from *above* 200 mb, it is possible that our simple two-layer simulation of the basic state is not capable of representing these processes.

The latitudinal distributions of AE and KE appear in figure 25. Both seasons show a larger energy content north of the Equator than they do south of the Equator.

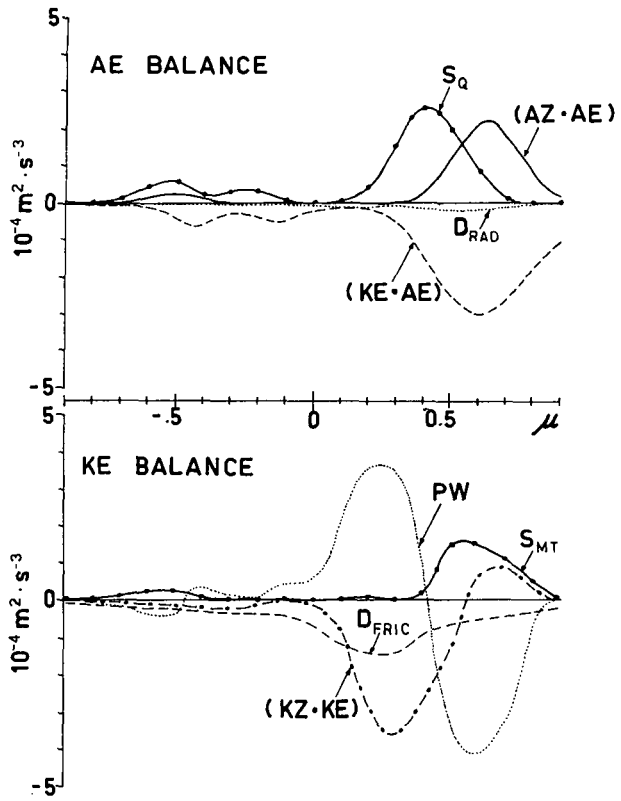

FIGURE 23.—Energy balance of the two-layer model with the basic state DJF due to forcing by the DJF heating field and orography.

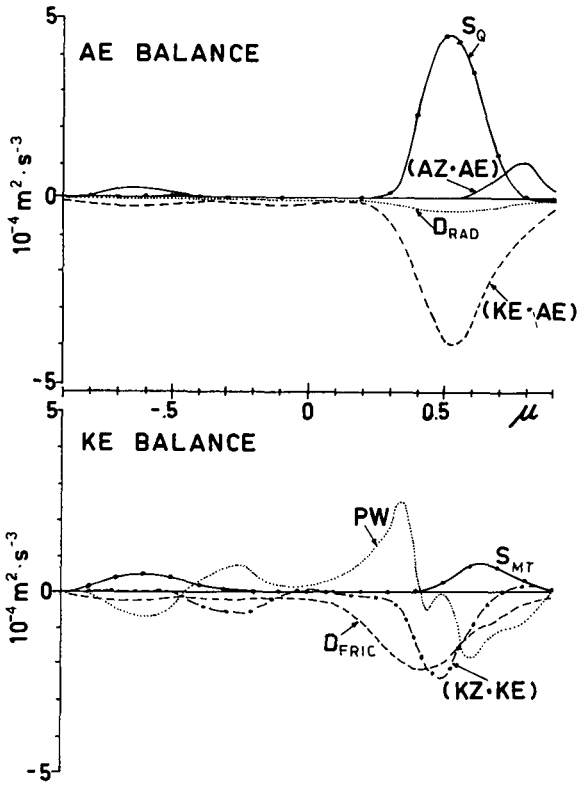

FIGURE 24.—Same as figure 23 for JJA.

This is consistent with the distributions of the two source terms, S_Q and S_{MT}, and the manner in which the energy tends to redistribute itself. Estimates (black dots) of the KE by Kidson (1968) are plotted upon the seasonal

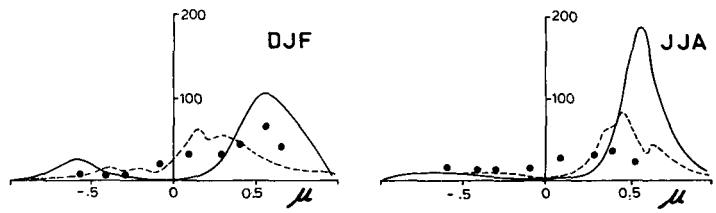

FIGURE 25.—Distribution of AE and KE ($m^2 \cdot s^{-2}$) for the two seasonal cases as a function of the sine of latitude, μ. The dots represent the observed values of Kidson (1968).

curves. These estimated values also show the same distinction between the two hemispheres. The results are especially compatible for DJF but are only fair for JJA.

Manabe et al. (1970), hereafter referred to as M, have made a comprehensive study of the energetics for January with particular emphasis on the low latitudes. Even though there is a large difference in the sophistication between the linear and nonlinear models and a slight difference in the definition of quantities, a comparison of the various statistics is most interesting. The corresponding eddy kinetic energy balances are shown in figure 23 of this study and figure 6.1 of M.

The KE balances show two main differences. The first difference is the relative simplicity of the energetics of the linear model compared with the distributions shown in M, probably a result of the simple basic state of the linear model and the neglect of extratropical forcing. The second difference occurs in the distribution of the (KZ·KE) term. In M, the conversion was found to be large and positive in the low latitudes of the Northern Hemisphere, in good agreement with the observations of Kidson et al. (1969). This large, positive conversion is due to the large southern transport of angular momentum across the Equator above 200 mb, which our model fails to predict.

The correspondence between the two estimates of the PW effect and the (AE·KE) conversion distributions (the "pressure interaction" and "eddy conversion" terms in M) is somewhat better. Overall, both models predict a maximum convergence of wave energy in the subtropics (although the maximum predicted by our linear model is slightly closer to the Equator) and a divergence in extratropical regions. Both models predict (AE·KE) maxima in roughly the same region, although the relative differences in magnitudes of the conversions between the two hemispheres is larger in the linear model.

The significance of the relative magnitudes of the PW and the (AE·KE) terms in the KE budgets of the equatorial regions is discussed at length in M. The ratio of these two terms signifies the relative importance of the local generation of KE compared to the remote generation of KE. In M, the interest was in determining the relative roles of lateral coupling with midlatitudes (the remote forcing) and condensational heating at low latitudes (the local forcing). From their figure 6.1, one can see that from 25° to 10°N the PW effect outweighs the (AE·KE) conversion, signifying the dominance of remote forcing. South of 10°N, the local KE source is far larger than the remote effect. From this, M concluded that the principle

source of KE at very low latitudes is condensational heating.

Because of the neglect of midlatitude forcing, the interpretation of the ratio in our model is slightly different. The comparison of the two terms in low latitudes is really a comparison between local forcing by the release of latent heat and remote forcing by heating and orography in the subtropics. From figure 23, we see that in the Northern Hemisphere the PW effect is by far the larger process equatorward of about $\mu=0.4$ (23°N). In the Southern Hemisphere, the (AE·KE) contribution is larger, inferring the dominance ot the local heating effects.

The large magnitude of PW in the low latitudes of the Northern Hemisphere may be attributed to the orographic forcing of the Himalayas. As we have noted earlier, the model tends to overestimate the influence of the mountains. This occurs because the orography is incorporated through a simple linear boundary condition that requires that all flow must be over the mountain and does not allow for flow around the mountain. In the real atmosphere, the resultant flow would be a combination of the two effects so that the model tends to overestimate the excitation of the westerlies and, possibly, underestimate the excitation of the easterlies to some extent.

However, besides the possible overestimation of the PW term in the Northern Hemisphere, the comparison of the PW and (AE·KE) terms in the KE budget lends support to two conclusions regarding the maintenance of the steady flow at low latitudes. First, in the summer Tropics, the acquisition of KE through the (AE·KE) conversion (i.e., by the release of latent heat within the summer Tropics) is of greater importance than the effect of remote forcing (i.e., through the PW effect) from the winter hemisphere or from the subtropics of the summer hemisphere. Second, in the Tropics of the winter hemisphere, the opposite appears to be true and the effect of remote energy sources (through the PW effect) appears to dominate the flow. However, due to the manner in which the forcing functions poleward of 30° were treated in this model, further comparisons with the results presented in M cannot be made without explicitly including extratropical forcing.

7. DISCUSSION

By comparing the response of a simple two-layer model with observed data and results from more sophisticated models, we have managed to draw some tentative conclusions about the role played by forcing functions located *within* the tropical atmosphere. Similarity between the observed and computed fields was found to be generally near the Equator, with the most serious discrepancies occurring at the northern and southern extremities of the Tropics.

The discrepancies probably arise from the neglect of the influence of steady forcing functions located poleward of the Tropics. This is most apparent in the Northern Hemisphere in JJA where an observed anticyclonic circulation in the North Pacific Ocean is completely omitted by our model. Eliassen and Palm (1961) have shown that an equatorial wave-energy flux is associated with stationary midlatitude disturbances. We have also noted that the response of the Eastern Hemisphere of the model is in much better agreement with observations than it is in the Western Hemisphere. Possibly this agreement occurs because the dominating energy sources of the Eastern Hemisphere (the Himalayas and Indian Ocean heating region) lie between low latitudes and the influence of northern Asia. The influence of the steady extratropical forcing functions upon the Tropics is presently being considered.

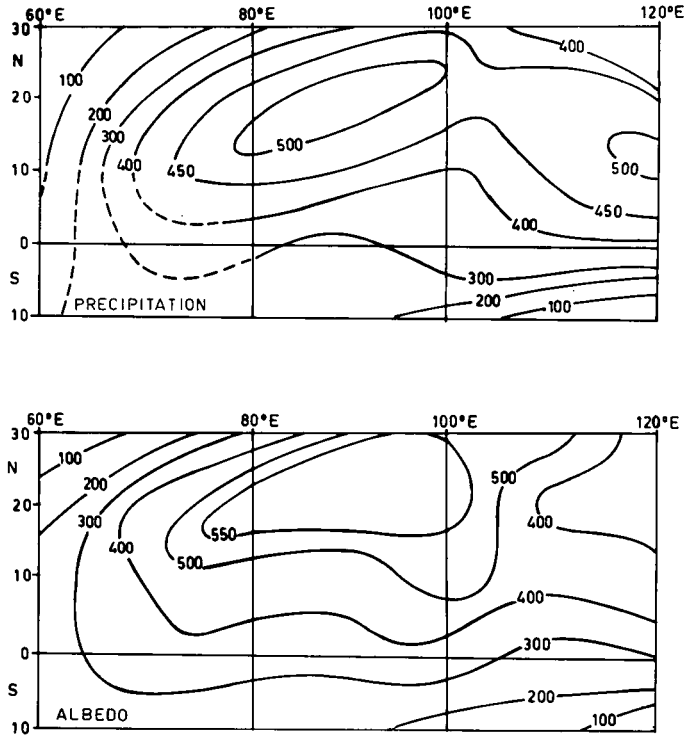

FIGURE 26.—Comparison of the latent heat estimates ($\mathcal{Q}_{LH}$) for the India–Indian Ocean region in JJA using precipitation data (upper diagram) and satellite albedo estimates (lower diagram). Dashed lines in the upper diagram represent interpolation in data-less areas. (Units are cal·cm^{-2}·day^{-1}.)

APPENDIX 1: COMPARATIVE EVALUATION OF THE LATENT HEAT ESTIMATES

Three areas, each possessing fair to good precipitation data coverage, are used for comparison with the latent heat estimates obtained in section 2. The areas consist of two continental regions, India and Africa, plus a section of the central Pacific Ocean. Mean precipitation distributions for JJA were used for the continental regions,[2] and an annual distribution was used for the ocean area (Jordan 1968).

The mean seasonal satellite albedo data compiled by Taylor and Winston (1968) are the mean of only one 3-mo period. However, the regions of maximum rainfall are also regions of minimum variability (Riehl 1954). We can, therefore, expect the brightness or albedo charts to

[2] The precipitation data used were compiled by the Massachusetts Institute of Technology Upper Atmosphere Project headed by R. E. Newell.

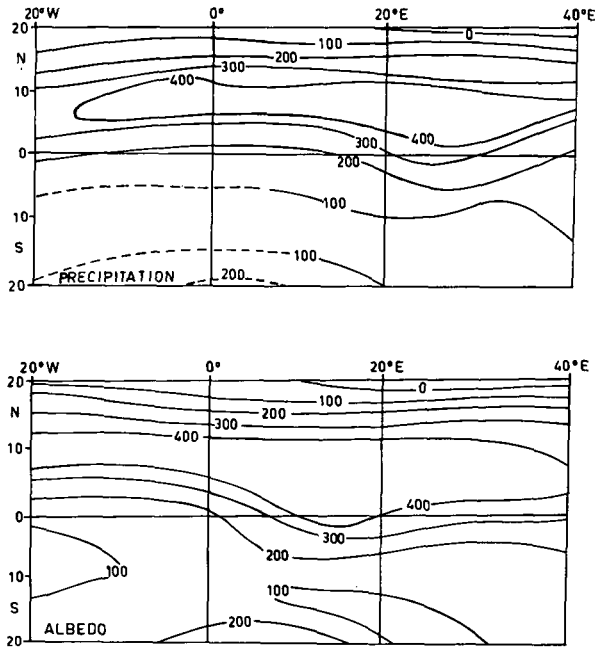

FIGURE 27.—Same as figure 26 for the equatorial African region in JJA.

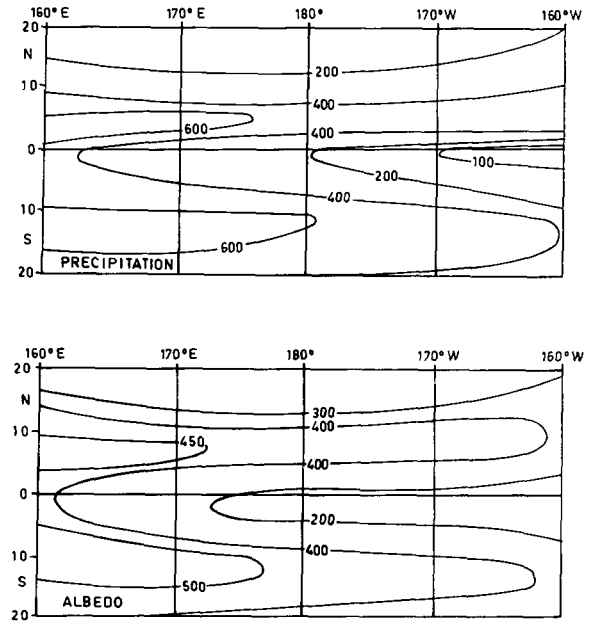

FIGURE 28.—Same as figure 26 for an annual mean in the Central Pacific region.

be representative of a longer term mean. The mean precipitation data, on the other hand, come from records of between 7 and 10 yr in length.

1. Isopleths of the total latent heat release in a unit column (cal · cm^{-2} · day^{-1}) for the two methods of estimation are shown for the Indian Ocean region (JJA) in figure 26. The dashed isopleths denote regions of poor data coverage. In general, there is fairly good correspondence over most of the region except for some difference in the northeast. The magnitudes are similar except for an apparent overestimate in the central area by about 10 percent.

2. The comparison for equatorial Africa (JJA) is shown in figure 27. Both distributions are dominated by a narrow intense maximum with a magnitude in excess of 400 cal · cm^{-2} · day^{-1} and a minimum region to the south. The main difference occurs in the magnitude of the minimum, which is overestimatsd considerably.

3. The comparison for the Marshall–Line Island region (annual mean) is shown in figure 28. The basic features are identical in each estimate, although the albedo method tends to underestimate the magnitude of the maxima by some 10–20 percent. The precipitation data from the island stations may not be representative of the area itself because of the interaction of the island with its environment. Since an island rainfall will always tend to be greater than the surrounding rainfall, this cannot explain why the minimum regions are once again overestimated.

In the three examples, the two estimates of the distribution of latent heat agree quite well. The magnitudes of the various maxima are also quite similar. The major difference lies with the magnitude of the minimum regions; this difference is most likely due to the effect of nonprecipitating clouds. However, the agreement is generally quite fair and allows us to use the latent-heat forcing functions with some confidence.

APPENDIX 2: DETERMINATION OF THE EIGENFUNCTIONS OF EQUATION (13)

Inspection of the coefficients of eq (9a) and (9b) suggests the separation

$$U^s,V^s,\Psi^s(\mu,Z)=U_s^*,V_s^*,\Psi_s^*(\mu)\alpha_s(Z)$$

and (42)

$$W^s(\mu,Z)=W_s^*(\mu)\beta_s(Z).$$

Using eq (42) in eq (9d) (homogeneous case, i.e., $q_s=0$), we obtain following relationships:

$$\alpha_s(Z)=P[\beta_s(Z)]$$

and (43)

$$\Psi_s^*(\mu)=\frac{W_s^*(\mu)}{\lambda_s E}$$

where E is the separation constant. Using eq (43), one can reduce eq (9) to

$$-\lambda_s U_s^*+A\mu V_s^*+s\Psi_s^*=0, \quad (44a)$$

$$-\lambda_s V_s^*+A\mu U_s^*+D(\Psi_s^*)=0, \quad (44b)$$

and

$$D(V_s^*)-sU_s^*+(1-\mu^2)\lambda_s E\Psi_s^*=0. \quad (44c)$$

Equation (44) constitutes the horizontal component of eq (9) and is identical to Laplace's tidal equations except for the definition of λ_s [Longuet-Higgins 1968, eq (7.2)]. Making use of this similarity, we can utilize Longuet-Higgins' results to determine the scale of E defined by the λ_s of our study. Two ranges of E were thus found. These were very large and positive and moderately large and negative.

Considering the eigenfunctions corresponding to $E>>0$, we eliminate U^* and Ψ^* from eq (44) to give an equation in V^* and follow Longuet-Higgins to seek the limit as $E\to\infty$. The equation becomes

$$\left[\frac{d^2}{d\eta^2}+(\lambda_s A E^{1/2})^{-1}(\lambda_s^3 E-sA-s^2\lambda_s)-\eta^2\right]V_s^*(\eta)=0 \quad (45)$$

where $\eta=A^{1/2}E^{1/4}\ \mu$. Equation (45) possesses solutions of the form

$$V^*_{n,s}(\eta_n)=H_n(\eta_n)\exp\left(\frac{-\eta_n^2}{2}\right) \tag{46}$$

if

$$\lambda_s^3 E-sA-s^2\lambda_s=\lambda_s AE^{1/2}(2n+1). \tag{47}$$

Here, H_n is the nth order Hermite polynomial. The remaining eigensolutions are

$$\begin{aligned} W^*_{n,s}(\eta_n)&=[C_1H_{n-1}(\eta_n)+C_2H_{n+1}(\eta_n)]\exp\left(-\frac{\eta_n^2}{2}\right),\\ \Psi^*_{n,s}(\eta_n)&=[C_3H_{n-1}(\eta_n)+C_4H_{n+1}(\eta_n)]\exp\left(-\frac{\eta_n^2}{2}\right),\\ \text{and}\qquad U^*_{n,s}(\eta_n)&=[C_5H_{n-1}(\eta_n)+C_6H_{n+1}(\eta_n)]\exp\left(-\frac{\eta_n^2}{2}\right) \end{aligned} \tag{48}$$

where the coefficients, C_i, are functions of n, s, E, and A. The orthogonality of the $W^*_{n,s}\ (\eta_n)$ is assumed from the orthogonality of their parent Hough functions.

Both Matsuno (1966) and Longuet-Higgins (1968) considered the possibility of a special mode with $V=0$ that is not taken into account in the former procedure. Setting $V=0$ in eq (44), one obtains the equation

$$\frac{dW^*}{d\mu}+\frac{A_s}{\lambda_s}\mu W^*=0 \tag{49}$$

and the condition

$$\lambda_s=\pm\frac{s}{E^{1/2}}. \tag{50}$$

In η-space, the solution of eq (49) may be written as

$$W^*(\eta)=\exp\left(-\frac{\eta^2}{2}\right), \tag{51a}$$

which, in turn, gives

$$\Psi^*(\eta)=\frac{\exp\left(-\frac{\eta^2}{2}\right)}{sE^{1/2}} \tag{51b}$$

and

$$U^*(\eta)=\frac{\exp\left(-\frac{\eta^2}{2}\right)}{s}. \tag{51c}$$

In the above procedure, the negative root of eq (50) is ignored to insure finiteness at $\eta=\pm\infty$. Matsuno (1966) has shown that eq (50) is also obtainable by setting $n=-1$ in eq (47). If we realize that $H_n(\eta)=0$ for $n<0$, then the solutions [eq (51)] may be included in the family [eq (46) and (48)].

For the forced problem, the eigenvalues may be evaluated from eq (47) since λ_s is a known function of δ and s. For $\delta<0$, eq (47) becomes

$$E_{n,s}=\frac{4A^2}{s^4|\delta|^4}\left\{(2n+1)\pm\left[(2n+1)^2+\frac{2s^2}{A}|\delta|+\frac{s^4}{A^2}|\delta|^2\right]^{1/2}\right\}^2. \tag{52}$$

To ensure finiteness of the solutions at $\eta=\pm\infty$, we chose the positive root; otherwise, $E^{1/2}_{n,s}<0$ and the exponents of the solution [eq (49)] would be positive. By letting $s\to\infty$, we see that for all n, $E\to 4/\delta^2$ [eq (50)].

Finally, we can write down the general eigensolutions. Using eq (8) and (14), we obtain

$$\begin{aligned} &\dot{Z},\ u,\ \psi,\ v(\varphi,\ \eta,\ Z)\\ &\quad=\sum_n\sum_s W^*_{n,s}(\eta)g_1^s(\varphi,\ Z),\ U^*_{n,s}g_2^s,\ \Psi^*_{n,s}g_2^s,\ V^*_{n,s}g_3^s \end{aligned} \tag{53}$$

where $W^*_{n,s}$, $U^*_{n,s}$, $\Psi^*_{n,s}$, and $V^*_{n,s}$ are given by eq (48) and (52) and

$$\begin{aligned} g_1^s(\varphi,\ Z)&=[Y_R(Z)\sin s\varphi+Y_I(Z)\cos s\varphi]\exp\left(\frac{Z}{2}\right),\\ g_2^s(\varphi,\ Z)&=[R_1(Y_R)\cos s\varphi+R_1(Y_I)\sin s\varphi]\exp\left(\frac{Z}{2}\right),\\ \text{and}\qquad g_3^s(\varphi,\ Z)&=[R_1(Y_R)\sin s\varphi+R_1(Y_I)\cos s\varphi]\exp\left(\frac{Z}{2}\right) \end{aligned} \tag{54}$$

where

$$R_1=\frac{d}{dZ}-\frac{1}{2}.$$

$Y_R(Z)$ and $Y_I(Z)$ represent the real and imaginary parts of the solution of the vertical structure equation [eq (15)]. The $(n,\ s)$ subscripts have been omitted for simplicity.

APPENDIX 3: REDUCTION OF EQUATION (27)

The finite-difference system used is a one-dimensional version of the "staggered centered-difference" scheme described by Phillips (1962). With this method, the meridional velocity components are expressed at each gridpoint while the other variables (U_i, Ψ_i, and ω) are expressed at points situated halfway between ("half-points"). This minimizes the truncation error by allowing the evaluation of the derivatives at the same point as the other variables.

These equations of the set containing derivatives in V are expressed at the half-points $(k+\frac{1}{2})$ while the remainder are written at the gridpoints (k). This procedure produces the following first-order difference equations:

$$\begin{aligned} n_1^{k+1/2}U_1^k+\tfrac{1}{2}n_2^{k+1/2}(V_1^k+V_1^{k+1})+l^{k+1/2}n_3^{k+1/2}(V_1^{k+1}-V_1^k)\\ +iK_2U_2^k=-s\Psi_1^k, \end{aligned} \tag{55a}$$

$$\tfrac{1}{2}n_5^k(U_1^{k-1}+U_1^k)+n_4^kV_1^k-K_2V_2^k=-l^k(\Psi_1^k-\Psi_2^{k-1}), \tag{55b}$$

$$\begin{aligned} iK_2U_1^k+\tfrac{1}{2}m_2^{k+1/2}(V_2^k+V_2^{k+1})+l^{k+1/2}m_3^{k+1/2}(V_2^{k+1}-V_2^k)\\ +m^{k+1/2}U_2^k=-s\Psi_2^k-F_1^{k+1/2}, \end{aligned} \tag{55c}$$

$$\tfrac{1}{2}m_5^k(U_2^{k-1}+U_2^k)+m_4^kV_2^k-K_2V_1^k=-l^k(\Psi_2^k-\Psi_2^{k-1}), \tag{55d}$$

$$s(U_1^k+U_2^k)-il^{k+1/2}(V_1^{k+1}+V_2^{k+1}-V_1^k-V_2^k)=F_2^{k+1/2}, \tag{55e}$$

and

$$\begin{aligned} s\bar{S}U_1^k+\tfrac{1}{2}j_2^{k+1/2}(V_1^{k+1}+V_2^{k+1}+V_1^k+V_2^k)-i\bar{S}l^{k+1/2}(V_1^{k+1}-V_1^k)\\ =j_1^{k+1/2}(\Psi_2^k-\Psi_1^k)+ij_2^{k+1/2}F_3^{k+1/2} \end{aligned} \tag{55f}$$

where the coefficients l^k, j^k, m^k, and n^k are complex functions of s, k, A_1, A_2, B, C, K_1, K_2, and K_3.

Equation (55) is reduced to a pair of coupled equations in V_1 and V_2 by a relatively straightforward process. First, Ψ_1 and Ψ_2 are obtained from eq (55a) and (55c) and used to eliminate the geopotential from the remainder of the set. Next, U_1 is eliminated using the modified thermodynamic equation. Finally, U_2 is eliminated using the remaining equations. We then have eq (29). After solving eq (29), the exact reverse procedure is used to obtain U_2, U_1, Ψ_2, and Ψ_1, respectively. Then, ω is obtained from the continuity equation.

ACKNOWLEDGMENTS

The author expresses his gratitude to Norman Phillips for his guidance and stimulation during the course of this study. Thanks are also due R. E. Newell and members of project AT(30–1) 2241 AEC for use of their low-latitude data.

This paper represents part of a thesis submitted in partial fulfillment of the doctoral requirements at the Massachusetts Institute of Technology.

The author also acknowledges support from the National Science Foundation under Grant No. GA–402X, the Commonwealth Bureau of Meteorology of Australia, and the Commonwealth Meteorology Research Centre, Melbourne, Australia, for the use of their facilities in compiling this manuscript.

REFERENCES

Berkofsky, Louis, and Bertoni, Eugene A., "Mean Topographic Charts for the Entire Earth," *Bulletin of the American Meteorological Society*, Vol. 36, No. 7, Sept. **1955**, pp. 350–354.

Bjerknes, Jakob A., "Atmospheric Teleconnections From the Equatorial Pacific," *Monthly Weather Review*, Vol 97, No. 3, Mar. **1969**, pp. 163–172.

Budyko, M. I. (Editor), *"Atlas Teplovago Balansa"* (Atlas of Thermal Balance), Glavnaia Geofizcheskaia Observatoriia, Leningrad, U.S.S.R., **1955**, 41 pp.

Charney, Jule G., "On the General Circulation of the Atmosphere," *The Atmosphere and the Sea in Motion*, Rockefeller Institute Press, New York, N.Y., **1959**, pp. 178–193.

Charney, Jule G., "A Note on Large-Scale Motions in the Tropics," *Journal of the Atmospheric Sciences*, Vol. 20, No. 6, Nov. **1963**, pp. 607–609.

Charney, Jule G., "The Intertropical Convergence Zone and the Hadley Circulation of the Atmosphere," *Proceedings of the WMO/IUGG Symposium on Numerical Weather Prediction, Tokyo, Japan, November 26–December 4, 1968*, Japan Meteorological Agency, Tokyo, Mar. **1969**, pp. III–73—III–79.

Charney, Jule G., and Drazin, P. J., "Propagation of Planetary-Scale Disturbances From the Lower Into the Upper Atmosphere," *Journal of Geophysical Research*, Vol. 66, No. 1, June **1961**, pp. 83–109.

Charney, Jule G., and Eliassen, Arnt, "A Numerical Method for Predicting the Perturbations in the Middle-Latitude Westerlies," *Tellus*, Vol. 1, No. 1, Stockholm, Sweden, May **1949**, pp. 38–54.

Dickinson, Robert E., "Propagators of Atmospheric Motions: Pt. 1. Excitation by Point Impulses," *Reviews of Geophysics*, Vol. 7, No. 3, Aug. **1969**, pp. 483–514.

Eliassen, Arnt, and Palm, Enok "On the Transfer of Energy in Stationary Mountain Waves," *Geofysiske Publikasjoner*, Vol. 22, No. 3, Oslo, Norway, Sept. **1961**, 23 pp.

Flattery, T. W., "Hough Functions," *Technical Report* No. 21, Department of the Geophysical Sciences, The University of Chicago, Ill., Mar. **1967**, 175 pp.

Flohn, Hermann, "Investigations on the Tropical Easterly Jet," *Bonner Meteorologische Abhandlungen*, No. 4, Bonn, Germany, **1964**, 83 pp.

International Business Machines Corp., "IBM Application Program: System/360 Scientific Subroutine Package (360A–CM–03X) Version III," *Document*, No. H20–0205–03, IBM Technical Publications Department, White Plains, N.Y., **1968**, pp. 337–341.

Johnson, D. H., "The Role of the Tropics in the Global Circulation," *The Global Circulation of the Atmosphere*, Royal Meteorological Society, London, England, Aug. **1969**, pp. 113–136.

Jordan, Charles L., Department of Meteorology, Florida State University, Tallahassee, **1968** (unpublished study).

Katayama, A. "On the Heat Budget of the Troposphere Over the Northern Hemisphere," Ph. D. thesis, Tohoku University, Japan, **1964**.

Kidson, John W., "The General Circulation of the Tropics," Ph. D. thesis, Massachusetts Institute of Technology, Cambridge, Mass., Sept., **1968**, 205. pp.

Kidson, John W., Vincent, Dayton G., and Newell, Reginald E., "Observational Studies of the General Circulation of the Tropics: Long Term Mean Values," *Quarterly Journal of the Royal Meteorological Society*, Vol. 95, No. 404, London, England, Apr. **1969**, pp. 258–287.

Koteswaram, P., "The Easterly Jet Stream in the Tropics," *Tellus*, Vol. 10, No. 1, Stockholm, Sweden, Feb. **1958**, pp. 43–57.

Krishnamurti, T. N., "Observational Study of Tropical Upper Tropospheric Motion Field During Northern Hemisphere Summer," *Report* No. 70–4, ESSA Grant E 22–64–68(G) Department of Meteorology, Florida State University, Tallahassee, Sept. **1970**, 51 pp.

Lindzen, Richard D., "Planetary Waves on Beta-Planes," *Monthly Weather Review*, Vol. 95, No. 7, July **1967**, pp. 441–451.

Lindzen, Richard D., "Internal Equatorial Planetary-Scale Waves in Shear Flow," *Journal of the Atmospheric Sciences*, Vol. 27, No. 3, May **1970**, pp. 394–407.

Longuet-Higgins, M. S., "The Eigenfunctions of Laplace's Tidal Equations Over a Sphere," *Philosophical Transactions of the Royal Society of London*, Ser. A, Vol. 262, No. 1132, England, Feb. 29, **1968**, pp. 511–607.

Mak, Man-Kin, "Laterally Driven Stochastic Motions in the Tropics," *Journal of the Atmospheric Sciences*, Vol. 26, No. 1 Jan. **1969**, pp. 41–64.

Manabe, Syukuro, and Smagorinsky, Joseph, "Simulated Climatology of a General Circulation Model With a Hydrologic Cycle: II. Analysis of the Tropical Atmosphere," *Monthly Weather Review*, Vol. 95, No. 4, Apr. **1967**, pp. 155–169.

Manabe, Syukuro, Holloway, J. Leith, Jr., and Stone, Hugh M., "Tropical Circulation in a Time-Integration of a Global Model of the Atmosphere," *Journal of the Atmospheric Sciences*, Vol. 27, No. 4, July **1970**, pp. 580–613.

Matsuno, Taroh, "Quasi-Geostrophic Motions in the Equatorial Area," *Journal of the Meteorological Society of Japan*, Ser. 2, Vol. 44, No. 1, Tokyo, Feb. **1966**, pp. 25–43.

Newell, Reginald E., Kidson, John W., Vincent, Dayton G., and Baer, George J., *The General Circulation of the Tropical Atmosphere and Interactions With Extra-Tropical Latitudes*, M. I. T. Press, Massachusetts Institute of Technology, Cambridge, Mass., **1972** (in press).

Phillips, Norman A., "The General Circulation of the Atmosphere: A Numerical Experiment," *Quarterly Journal of the Royal Meteorological Society*, Vol. 82, No. 352, London, England, Apr. **1956**, pp. 123–164.

Phillips, Norman A., "Numerical Integration of the Hydrostatic System of Equations With a Modifield Version of the Eliassen Finite-Difference Grid," *Proceedings of the International Symposium on Numercial Weather Prediction, Tokyo, Japan, November 7–13, 1960*, Meteorological Society of Japan, Tokyo, Mar. **1962**, pp. 109–120.

Phillips, Norman A., "Geostrophic Motion," *Reviews of Geophysics*, Vol. 1, No. 2, May **1963**, pp. 123–176.

Ramage, C. S., "Role of a Tropical 'Maritime Continent' in the Atmospheric Circulation," *Monthly Weather Review*, Vol. 96, No. 6, June **1968**, pp. 365–370.

Riehl, Herbert, *Tropical Meteorology*, McGraw-Hill Book Co., Inc., New York, N.Y., **1954**, 392 pp.

Riehl, Herbert, "Varying Structure of Waves in the Easterlies," *Proceedings of the International Symposium of Large-Scale Atmospheric Processes, Moscow, U.S.S.R., June 23–30*, **1965**, Izdatvo Nauka, Moscow, **1965**, pp. 411–416.

Rossby, Carl-Gustav, and others, "Relations Between Variations in the Intensity of the Zonal Circulation of the Atmosphere and the Displacements of the Semi-Permanent Centers of Action," *Journal of Marine Research*, Vol. 2, No. 1, **1939**, pp. 38–55.

Smagorinsky, Joseph, "The Dynamical Influence of Large-Scale Heat Sources and Sinks on the Quasi-Stationary Mean Motions of the Atmosphere," *Quarterly Journal of the Royal Meteorological Society*, Vol. 79, No. 341, London, England, July **1953**, pp. 342–366.

Taylor, V. Ray, and Winston, Jay S., "Monthly and Seasonal Mean Global Charts of Brightness From ESSA 3 and ESSA 5 Digitized Pictures, Feb. 1967–Feb. 1968," *ESSA Technical Report* NESC 46, National Environmental Satellite Center, Washington, D.C., Nov. **1968**, 9 pp.

Thompson, Philip Duncan, *Numercial Weather Analysis and Prediction*, Macmillan Publishing Co., Inc., New York, N.Y., **1961**, 170 pp.

Vincent, Dayton G., "Seasonal Changes in the Global Atmospheric Energy Balance and Results for Restricted Regions," Ph. D. thesis, Massachusetts Institute of Technology, Cambridge, Mass., Nov., **1969**, 174 pp.

Yanai, Michio, and Maruyama, Takio, "Stratospheric Wave Disturbances Propagating Over the Equatorial Pacific," *Journal of the Meteorological Society of Japan*, Ser. 2, Vol. 44, No. 5, Tokyo, Oct. **1966**, pp. 291–294.

[*Received June 4, 1971; revised November 17, 1971*]

NOTICE TO AUTHORS

The Monthly Weather Review has begun requesting the author's organization to share the editorial production costs of his article by paying a charge of $40.00 per page. Rising costs have made this new policy necessary.

469-748 O - 72 - 4